Heavy oils and oil shales: Their shear story

Jyoti Behura[1], Mike Batzle[2] and Ronny Hofmann[2]
[1] *Center for Wave Phenomena, Colorado School of Mines, Golden, CO 80401*
[2] *Center for Rock Abuse, Colorado School of Mines, Golden, CO 80401*

ABSTRACT
Heavy oils and oil shales are important unconventional hydrocarbon resources with a huge potential. Multicomponent seismology can play an important role in monitoring these reservoirs at their various stages of development.
Most laboratory data are in the ultrasonic band, thereby limiting their use in seismic data analysis. Our measurements, acquired in the seismic band, can potentially be used directly in analyzing seismic data. We analyze a heavy-oil rock from Uvalde, Texas, and also the oil extracted from it, and also examine two oil shale samples, one with $\approx 30\%$ and another with $\approx 5\%$ organic content, from the Green River Formation, Colorado.
The modulus and quality factor (Q) of the heavy-oil rock shows a moderate dependence on frequency, but is strongly influenced by temperature. At room temperatures, the extracted heavy oil supports a shear wave, but with increase in temperature, its shear modulus decreases rapidly, which translates to a rapid drop in the shear modulus of the rock as well. At these low to intermediate temperatures (30°C-100°C), an attenuation peak corresponding to the viscous relaxation of the heavy oil is encountered. At yet higher temperatures, the lighter components of the heavy oil are lost, making the oil stiffer and less attenuative, which again translates to similar behavior of the heavy-oil rock.
Both the kerogen-rich and the lean shale show a weak dependence of modulus and Q on frequency. Their properties can be effectively considered frequency independent within the seismic bandwidth. These shales, however, show a dramatic change in shear-wave velocity and attenuation with temperature. Their shear moduli and Q decrease with melting of the kerogen, but with the subsequent loss of some of the kerogen, both shear moduli and Q increase. The magnitudes of these changes along the direction of the bedding and perpendicular to the bedding differ, which makes velocity anisotropy and attenuation anisotropy potentially valuable parameters. As the weak layers (kerogen) in shales influence the bedding-perpendicular properties more than they do the bedding-parallel properties, the melting and subsequent evaporation of kerogen change the velocity anisotropy and attenuation anisotropy of the shales significantly, in some cases by more than an order of magnitude. The amount of kerogen content in a shale also influences the velocity and attenuation. The more the organic content, the lower is the shear modulus and the higher the attenuation.
The dramatic changes in velocities and attenuation in heavy oils and oils shales should be clearly visible is seismic data, offering the promise that these measurements can be qualitatively and quantitatively used in seismic analysis.

Key words: Heavy oil, oil shale, attenuation, quality factor, shear modulus, anisotropy

Introduction

High oil prices have focused new interest on 'unconventional' hydrocarbon sources: heavy oil and oil shales. These energy resources have reserves that are nearly triple the world reserves of conventional oil and gas.

Heavy oil is a type of crude oil that is highly viscous and therefore does not flow easily. The US Department of Energy defines heavy oil as oil with API gravities between 10.0° and 22.3°, although the exact relation between API gravity and viscosity is not clear. The common characteristic properties are high specific gravity, low hydrogen-to-carbon ratio, high carbon residue, and high content of asphaltenes, heavy metal, sulfur, and nitrogen. It is believed that crude originally is not heavy but a variety of biological (bacterial action), chemical, and physical processes degrade it into heavy oil (Curtis et al., 2002). Heavy oil reservoirs are typically found in geologically young formations - Pleistocene, Pliocene, and Miocene. The largest known deposits are in the Athabasca sands in Canada, Faja del Orinoco in Venezuela, Utah, California, and Duri field in Indonesia (Curtis et al., 2002). The major challenge in exploiting heavy oil comes from its high viscosity, which makes production and transportation a costly affair. Cold production of heavy oil from a reservoir usually has a recovery efficiency of less than 10%. Steamflooding, the most common recovery process followed by the industry, has a recovery efficiency as high as 80%. New drilling technologies such as steam-assisted gravity drainage (SAGD) have also assisted in increasing the recovery.

Steamflooding and production change physical properties, such as velocity, density, and attenuation, of a formation. These changes can potentially be inferred from time-lapse studies, thereby helping in reservoir monitoring, as suggested by Nur et al. (1984). Recovery efficiency can be improved by monitoring the steamflood remotely using time-lapse seismic studies as done in Duri field, Indonesia (Jenkins et al., 1997). Watson et al. (2001) used traveltime-based methods to delineate areas of steam injection while Hedlin et al. (2001) found seismic-attenuation anomalies consistent with areas of steam injection. Schmitt (1999) observed significant difference between the sonic log velocities and VSP interval velocities within a heavy oil sand reservoir (Figure 1). Understanding such properties of these materials is essential to effective monitoring, since under some conditions the material acts like a solid, while under other conditions, like a liquid.

Laboratory measurements are necessary to understand the physical changes that accompany heating of heavy oil rocks. Not many laboratory studies, however, have been carried out. Nur et al. (1984) studied the influence of temperature on the velocities and attenuation of glycerol-filled Boise sandstones and on oil sands. Han et al. (2005) looked at the shear-wave velocity in heavy oils. Batzle et al. (2004, 2005) have also measured velocities and attenuation in heavy oils. Most of the above laboratory measurements are ultrasonic and results do not necessarily apply in the seismic band.

A vast unexploited source of hydrocarbons is oil shales, i.e., shales rich in kerogen. The Schlumberger Oilfield Glossary defines kerogen as "the naturally occurring, solid, insoluble organic matter that occurs in source rocks and can yield oil upon heating." Typical organic constituents of kerogen are algae and woody plant material. Kerogens have a high molecular weight relative to bitumen, or soluble organic matter. Bitumen forms from kerogen during petroleum generation. Estimates vary as to how many barrels of oil are contained in oil shale reserves. The US Office of Naval Petroleum and Oil Shale Reserves estimates there are some 1.6 trillion barrels of oil contained in oil shales around the world, with 60-70% of reserves (1.0-1.2 trillion barrels) in the United States. Most US oil shale is concentrated in the Green River Formation in Wyoming, Utah, and Colorado. These oil shale resources underlie a total area of 16,000 square miles (40,000 km^2). Technical challenges and environmental concerns, however, hinder their exploitation. Environmental considerations, for example, have rendered surface-mining unfeasible. This calls for in-situ recovery, which poses new technical challenges. The most promising in-situ project is being carried out by Shell Oil Company under the name of the Mahogany Research Project in Colorado, which uses electrical heating. A heating element is lowered into the well and allowed to heat the kerogen over time, slowly converting it into oils and gases, which are then pumped to the surface.

Seismic techniques can play an important role in monitoring changes in these oil shale reservoirs. Heating will change physical properties such as modulus, anisotropy, and attenuation, which can have a substantial effect on seismic wave propagation. The response of oil shales under varying temperature and pressure to seismic waves, however, is not well understood. To address this problem, experiments have been carried out under controlled conditions in the laboratory. Oil shales have been studied in the laboratory (Parker, 1968; Johnston, 1987; Mah, 2005) to understand their physical properties, including anisotropy. These studies, however, are limited to the ultrasonic band.

To understand the shear behavior of heavy-oil rocks and oil shale in the seismic frequency band, we conduct torsional experiments in these rocks to decipher their shear moduli and shear attenuation under varying temperature and frequency. For heavy oils, we examine both the rock containing the oil and the heavy oil extracted from the rock. When studying oil shales, we analyzed two samples of shale from the same formation (Green River Formation, Colorado) with different amounts of organic content. To our knowledge, no such studies with simultaneous change in temperature and frequency have yet been published in the geophysics community.

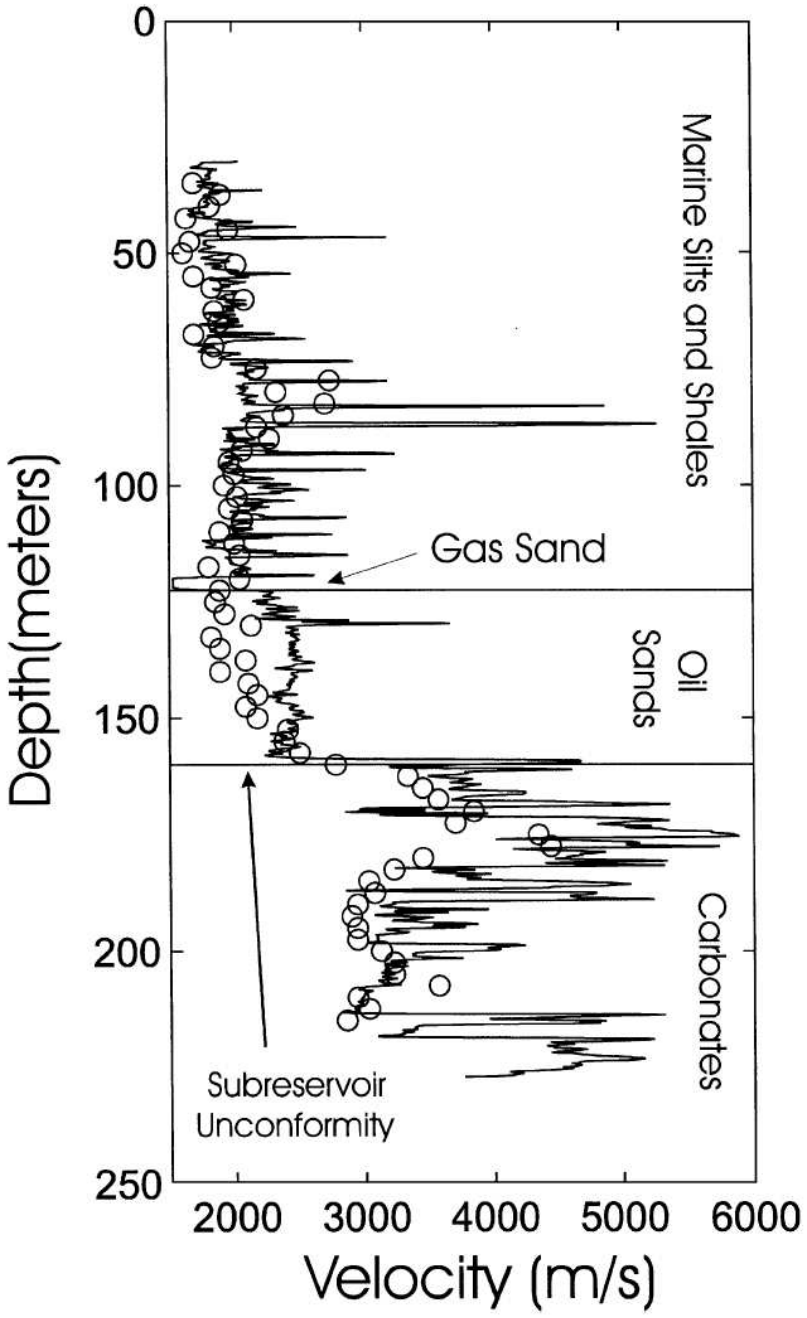

Figure 1. Sonic log velocities (line) and VSP interval velocities (open circles) in a well through oil sands (Schmitt, 1999).

1 THE EXPERIMENT

Measurements are carried out using a shear rheometer shown in Figure 2. The rock sample is clamped at both ends, and measurements are conducted with the sample dry and under no lateral confining stress. A sinusoidal torsional strain is applied on one end, and the resulting stress is recorded on the other end, which is fixed. The experiment is schematically shown in Figure 3. When a viscoelastic material is subjected to a sinusoidally varying strain, a steady state will be reached when the resulting stress is also sinusoidal, with the same angular frequency, but with a phase lag of δ, which is a measure

of attenuation of that body (O'Connell and Budiansky, 1978). For an elastic material, $\delta = 0$, and for a viscous fluid, δ can approach $\pi/2$, while δ for a viscoelastic body has a value between these two limits.

The strain, ϵ, and stress, σ, can be represented by

$$\epsilon = \epsilon_0 e^{-i\omega t}, \tag{1}$$

$$\sigma = \sigma_0 e^{-i(\omega t - \delta)}. \tag{2}$$

The above complex form of the stress function is divided by the strain to give the complex dynamic shear modulus, $\tilde{G}$,

$$\tilde{G} = \sigma_0'/\epsilon_0 + i\,\sigma_0''/\epsilon_0, \tag{3}$$

where

$$\sigma_0' = \sigma_0 \cos\delta, \tag{4}$$

$$\sigma_0'' = \sigma_0 \sin\delta. \tag{5}$$

The in-phase part of the stress, σ_0', gives the "real" or the "storage" modulus, G', and the out-of-phase part of the stress gives the "imaginary" or "loss" modulus, G'',

$$G' = \sigma_0'/\epsilon_0, \tag{6}$$

$$G'' = \sigma_0''/\epsilon_0. \tag{7}$$

The quality factor, Q, which is inversely proportional to the attenuation coefficient, is defined as (O'Connell and Budiansky, 1978)

$$Q \equiv 1/\tan\delta = 2\pi \frac{W_{st}}{W_{dis}}, \tag{8}$$

where W_{st} is the maximum elastic stored energy during a cycle of loading at the frequency under consideration and W_{dis} is the energy dissipated per cycle. The above definition of Q differs from the seismic quality factor (denoted as Q_S here) defined by Futterman (1962). O'Connell and Budiansky (1978) derived the relationship between Q and Q_S which is given as

$$Q_S = 2\pi\{1 - e^{-4\pi[(1+Q^2)^{1/2} - Q]}\}^{-1}. \tag{9}$$

From equation 9, when for $Q >> 1$, $Q_S \approx Q$, and when $Q \to 0$, $Q_S \to 2\pi$. Thus, for a Newtonian fluid, the shear wave $Q_S = 2\pi$ and $Q = 0$. In seismic studies, usually Q_S is calculated using the spectral ratio method, and can be converted to Q using equation 9. We will be using Q for all our results, and not Q_S.

W_{dis} can be calculated by integrating the out-of-phase component of stress over an entire cycle (Roylance, 2001):

$$W_{dis} = \int_0^{2\pi/\omega} (\sigma_0'' \sin\omega t)(-\epsilon_0 \omega \sin\omega t)dt, \tag{10}$$

$$= -\pi\sigma_0''\epsilon_0. \tag{11}$$

$$= -\pi G''\epsilon_0^2. \tag{12}$$

Equation 12 can be interpreted to imply that the energy supplied to the material by the out-of-phase components is irreversibly converted to heat. Similarly, integration of the in-phase components over the full cycle yields zero work, implying that energy associated with the in-phase components is reversible, so there is no loss of energy for the in-phase components for a full cycle. The maximum energy stored by the in-phase components occurs at a quarter of the cycle and is calculated as follows:

$$W_{st} = \int_0^{\pi/2\omega} (\sigma_0' \cos\omega t)(-\epsilon_0 \omega \sin\omega t)dt, \tag{13}$$

$$= -\frac{1}{2}\sigma_0'\epsilon_0. \tag{14}$$

$$= -\frac{1}{2}G'\epsilon_0^2. \tag{15}$$

The quality factor can now be calculated from equations 8, 12, and 15:

$$Q = \frac{1}{\tan\delta} = \frac{G'}{G''}. \tag{16}$$

2 HEAVY OIL ANALYSIS

We will describe the observations from the examination of heavy-oil rock and then move on to the results of analyzing the oil extracted from it.

2.1 Uvalde heavy-oil rock

Pictures of a rock sample from Uvalde, Texas, before and after heating, are shown in Figure 4. This carbonate has a porosity of $\approx$ 25% and permeability of 550 mD. The rock is examined under temperatures ranging from 30°C to 350°C with increments of 10°C. To understand the dispersion behavior, for each temperature, the sample is analyzed for frequencies ranging from 0.01 to 80 Hz (with increments of 0.1 on the log scale). All measurements are made in the linear viscoelastic regime, which is tested by conducting a strain-sweep experiment. In a strain-sweep experiment, the modulus of the rock is measured for increasing strain amplitudes. Within the linear viscoelastic regime, the modulus does not change; and a strain amplitude lying within this linear region is selected for conducting all other temperature-frequency measurements of the rock. For testing heavy-oil rocks and the extracted oil, we use a strain of $8\text{x}10^{-5}$. Note that this strain amplitude is larger than the strains encountered in exploration seismology, where the strains are around 10^{-6} (Winkler et al., 1979). As pointed out by Iwasaki et al. (1978), higher strain amplitudes might result in lower moduli. To verify the validity of this statement, further experiments have to be carried out at lower strain amplitudes. For the time being, we assume that the higher strain does

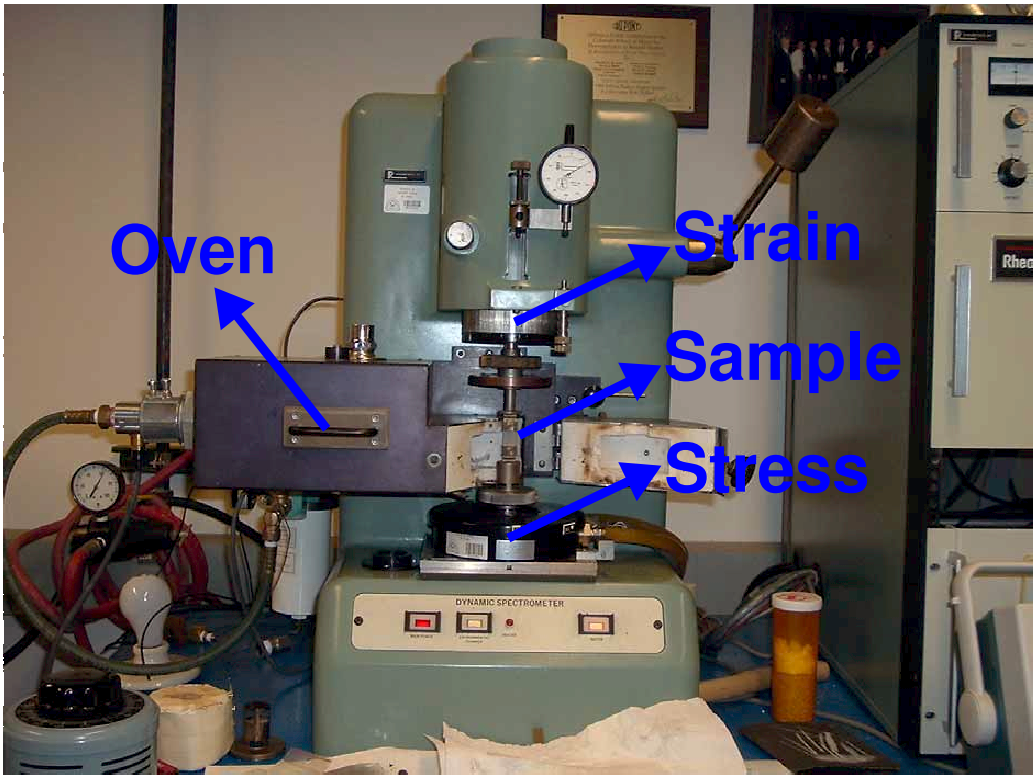

Figure 2. The rheometer used in the study (courtesy of Dr. John Dorgan, Chemical Engineering, CSM).

not significantly change the modulus and the relaxation mechanisms remain the same.

2.1.1 Observations

The storage modulus, G', and the loss modulus, G'', are shown in Figures 5a and 5b, respectively. The data has not been smoothed and is presented as it is without any processing; also none of the data, shown later, has been smoothed. G' increases with frequency for temperatures less than ≈150°C. At higher temperatures, however, the storage modulus has a weak dependence on frequency. The strong temperature dependence of G' can be clearly seen in Figure 5a. G' is highest (≈10 GPa) at room temperature, decreases rapidly with increasing temperature, attaining a minimum value at around 150°C (this temperature-minimum changes with frequency). With further rise in temperature, G' increases gradually to approximately 1.8 GPa at 350°C. Later, we will show how well these results match with shear-wave velocities measured in the field.

Figure 5c shows $1/Q$ of the rock and Q is shown in Figure 5d. Note the moderately strong dependence of attenuation on frequency . A relaxation mode can be seen at temperatures less than 100°C. This relaxation is characterized by an attenuation peak (Figure 5c) or a Q trough (Figure 5d). For example, at 70°C, the attenuation increases with increasing frequency, attains a peak at 1 Hz, and then drops with further increase in frequency. The position of the relaxation peak shifts towards higher frequencies with increasing temperature. The same attenuation peak can be better seen when plotted as a function of temperature for a particular frequency, as shown in Figure 6. Note that Q changes significantly with temperature. Q is roughly 5 at room temperature within the seismic band and decreases with increasing temperature, attaining a value as low as 3. Q is ≈ 6 at 80 Hz for temperatures greater than 200°C, which is close to the value observed ($Q_S = 10$ which corresponds to $Q = 6$) by Macrides and Kanasewich (1987) in the steam-invaded oil sands of Clearwater Formation in Alberta, Canada. With yet further increase in temperature, Q increases, reaching ≈ 40 at 350°C (Fig-

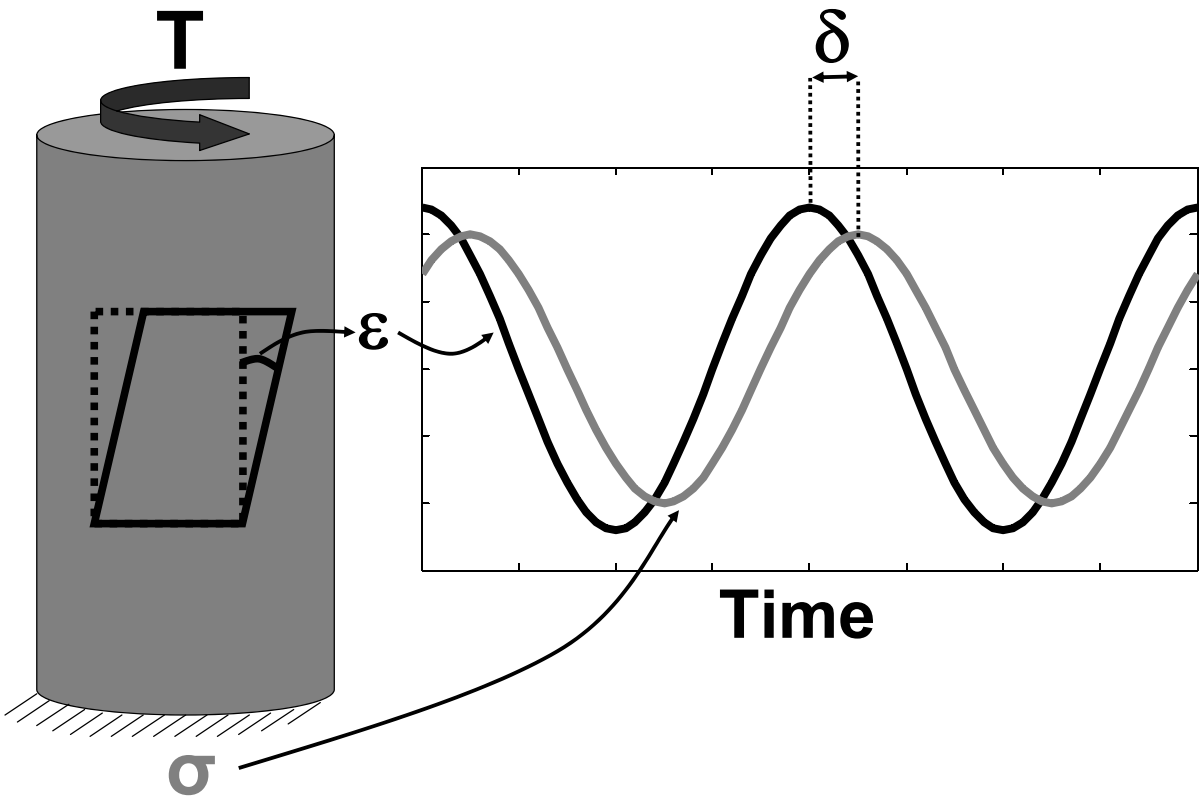

Figure 3. Schematic diagram of a harmonic loading applied to a rock sample. T denotes the torque applied to one end of the sample. The resulting stress (gray) lags behind the strain (black) by a phase angle δ.

ure 6). This is not seen in Figure 5d as the color scale has been modified to bring out the important trends in Q.

2.2 Extracted heavy oil

We examined the heavy oil under temperatures ranging from 30°C to 250°C with increments of 10°C, for the same frequency range as studied for the rock (0.01 to 80 Hz). All measurements are conducted in the linear viscoelastic regime for a strain of $8\text{x}10^{-5}$. The heavy oil moduli and quality factor are shown in Figures 7a-d. The heavy oil was measured under two different experimental arrangements - rectangular samples for low temperatures and thin-plate cylindrical samples for higher temperatures. This is necessary because at temperatures above $\approx$ 80°C, the rectangular sample does not retain its shape because of melting.

2.2.1 Observations

The storage modulus and the loss modulus are shown in Figures 7a and 7b, respectively. The trends observed for the mechanical properties of the rock are similar to those in the extracted oil. This supports that the behavior of the heavy oil within the rock dominates the mechanical response of the rock. The oil shows noticeable dispersion for temperatures less than $\approx$ 180°C (Figure 7a). At higher temperatures, however, the storage modulus is nearly constant with frequency. With increasing frequency, G' generally increases for all temperatures.

The strong temperature dependence of G' can be clearly seen from Figure 7a. G' is highest ($\approx$ 1.0 GPa) at room temperature in the seismic band and decreases rapidly with increasing temperature, attaining a minimum value at around $\approx$ 180°C (as for the rock, the value of this minimum and the temperature of its occurrence changes with frequency). With further rise in temperature, G' increases to about 0.002 GPa at 250°C.

The quality factor is shown in Figures 7c and 7d. As no trends are visible in Figures 7c, its color scale

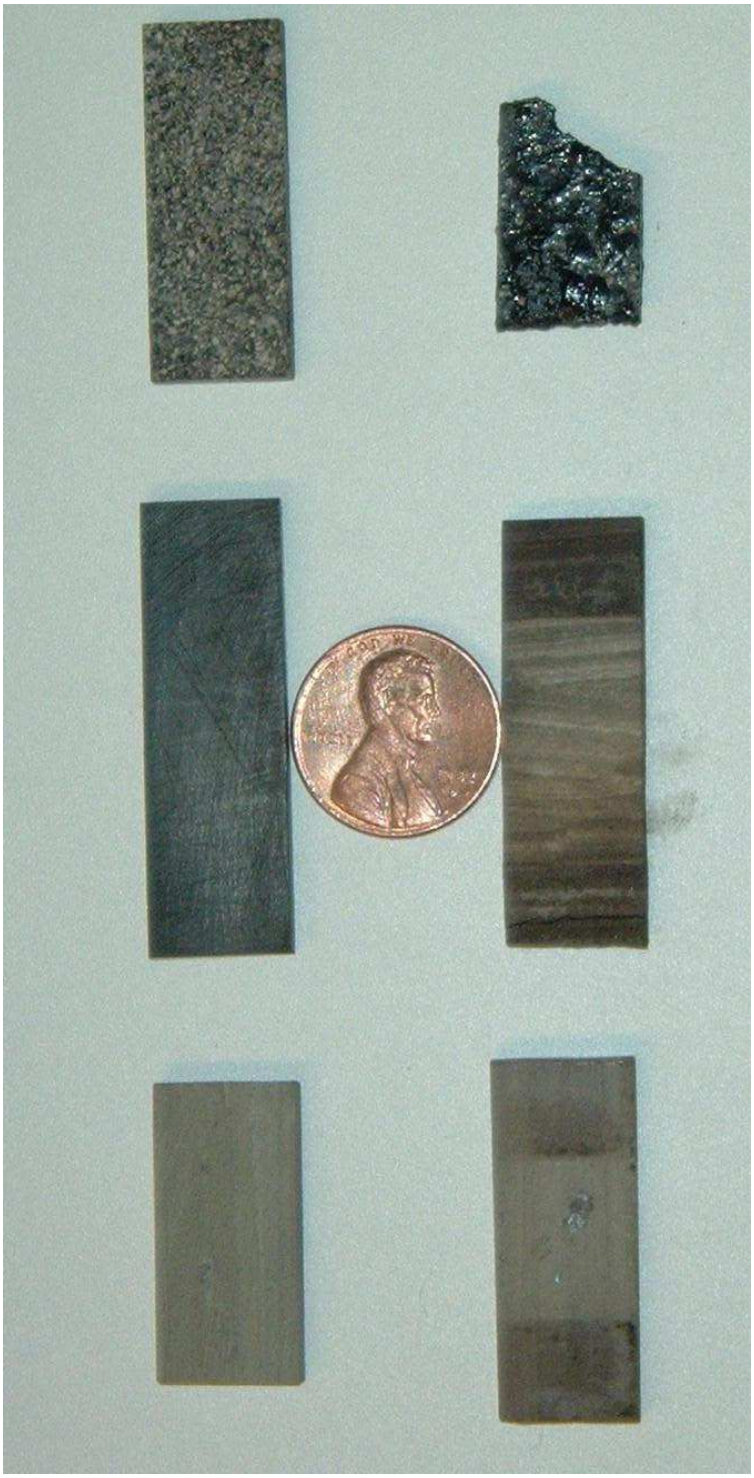

Figure 4. Before (left column) and after (right column) pictured of some samples used in the experiment - Uvalde heavy oil rock (top row), kerogen-rich shale (middle row), and lean shale (bottom row).

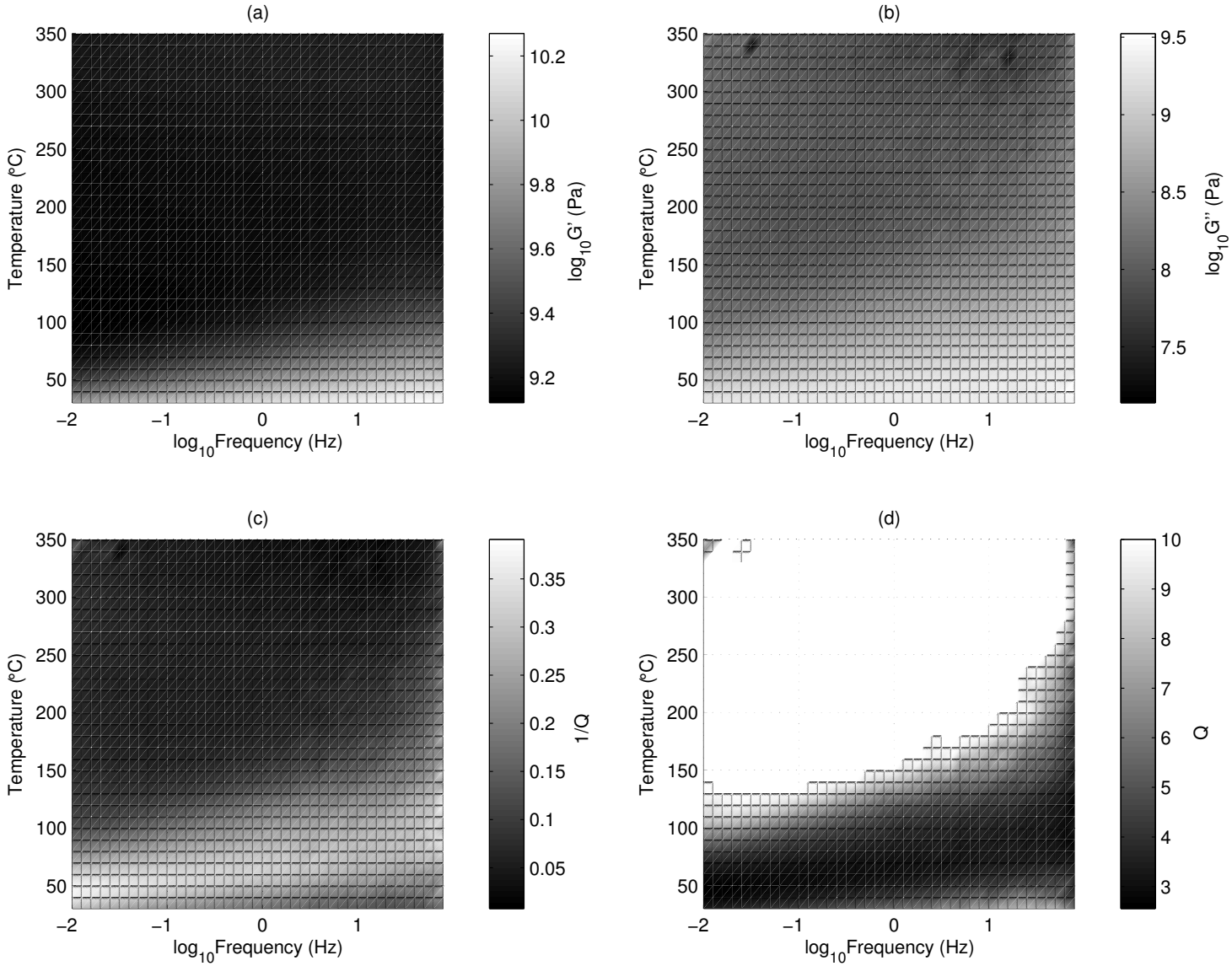

Figure 5: The shear (a) storage modulus G', (b) loss modulus G'', (c) $1/Q$, and (d) quality factor Q of Uvalde heavy oil rock. The color scale in (d) is modified to bring out the trends for Q. Measurements are done at increments of 10°C and frequency increments of 0.1 on the $\log_{10}$ scale.

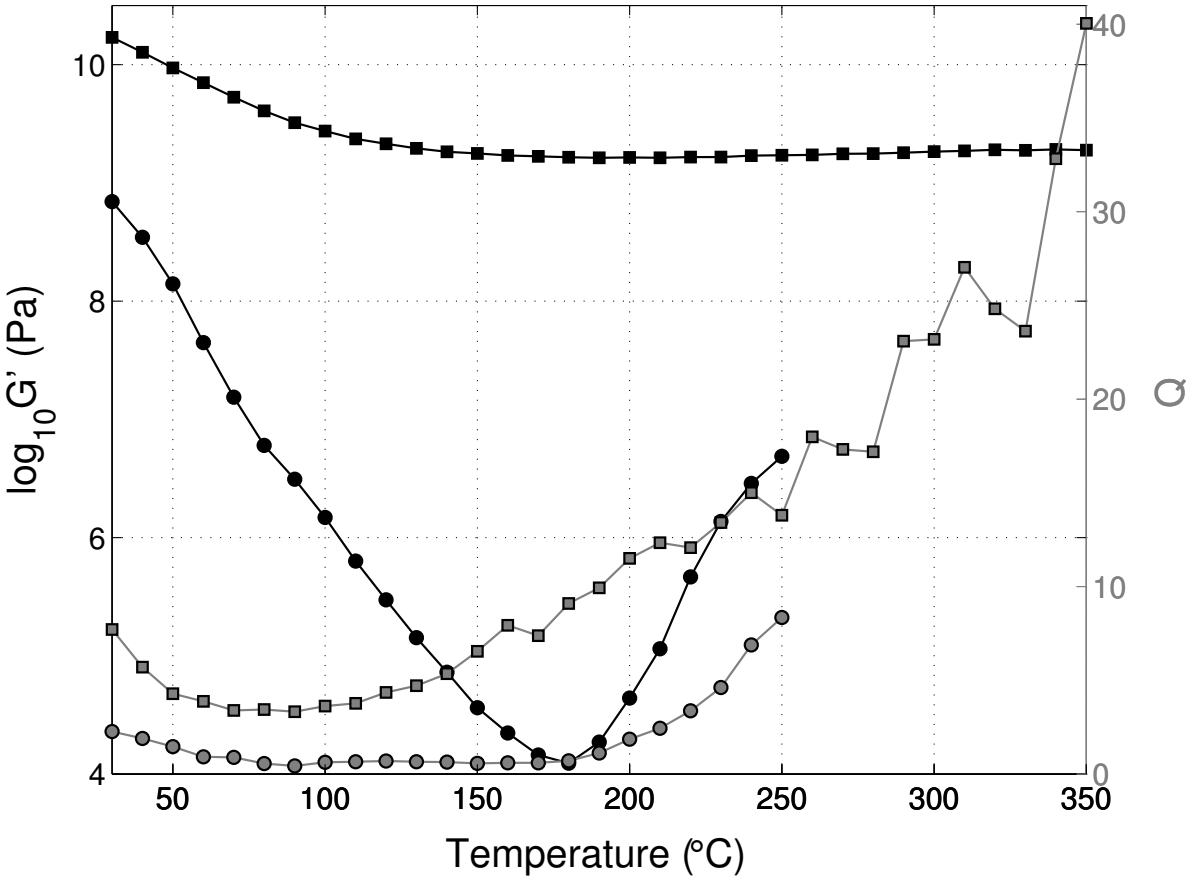

Figure 6. G' (black) and Q (gray) of Uvalde heavy-oil rock (squares) and the extracted heavy oil (circles) measured at 12.6 Hz.

is modified to bring out the trends and the resulting data is shown in Figure 7d. Q shows a moderately weak dependence on frequency, with some general increases with frequency. There seems to be a relaxation mechanism active in the temperature range of 50°C to 100°C, where Q initially decreases with frequency, reaches a trough, and then subsequently increases with further increase in frequency. The minimum Q in this region is close to 0. The position of this minimum shifts to higher frequencies with increasing temperature.

Not surprisingly, Q changes significantly with temperature. The quality factor of the oil is ≈ 2.5 at room temperature in the seismic band, and decreases with increase in temperature, attaining a value close to 0 as the oil goes through the relaxation mechanism. With yet further increase in temperature, Q initially increases and then drops before increasing again. This can be clearly seen at 0.01 Hz, where Q increases after the initial relaxation trough at 60°C (Figure 7d). At further higher temperatures, melting of the oil reduces Q, and it attains values as low as 0.2 at 140°C. With further heating, Q rises again.

2.3 Mechanisms

The strong temperature dependence of the modulus and the attenuation comes from the melting of the heavy oil and its subsequent composition change at high temperatures. Nur et al., (1984) suggested that this change in the heavy oil translates to a significant change in the mechanical response of the rock containing the heavy oil.

The increase in G' of the rock with frequency is consistent with the frequency dependence of G' of the heavy oil. Heavy oil is viscoelastic, and so at low frequencies, the molecules/chains in the viscoelastic material have time to slide relative to eachother, resulting in a low storage modulus. In contrast, at relatively higher frequencies the molecules/chains do not have sufficient time to slide as they are "locked", thereby making the material stiffer (high G'), as there is a

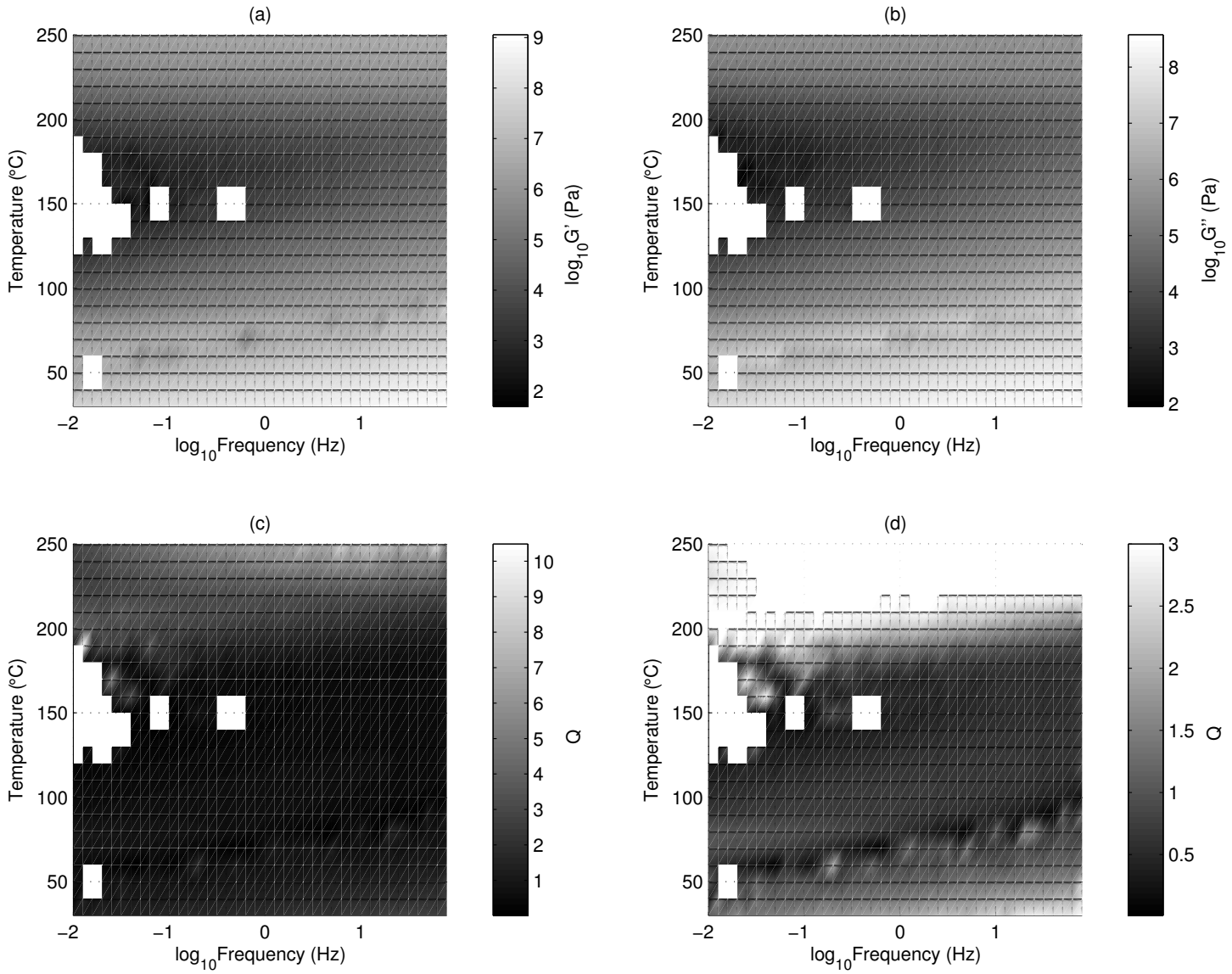

Figure 7: The shear (a) storage modulus (G'), (b) loss modulus (G''), and the (c) quality factor Q of the oil extracted from the Uvalde heavy oil rock. The color scale in (c) is modified in (d) to show the trends for Q. Measurements are done at increments of 10°C and frequency increments of 0.1 on the $\log_{10}$ scale. The missing data points correspond to erroneous results (e.g., negative moduli) arising from noise or experimental errors.

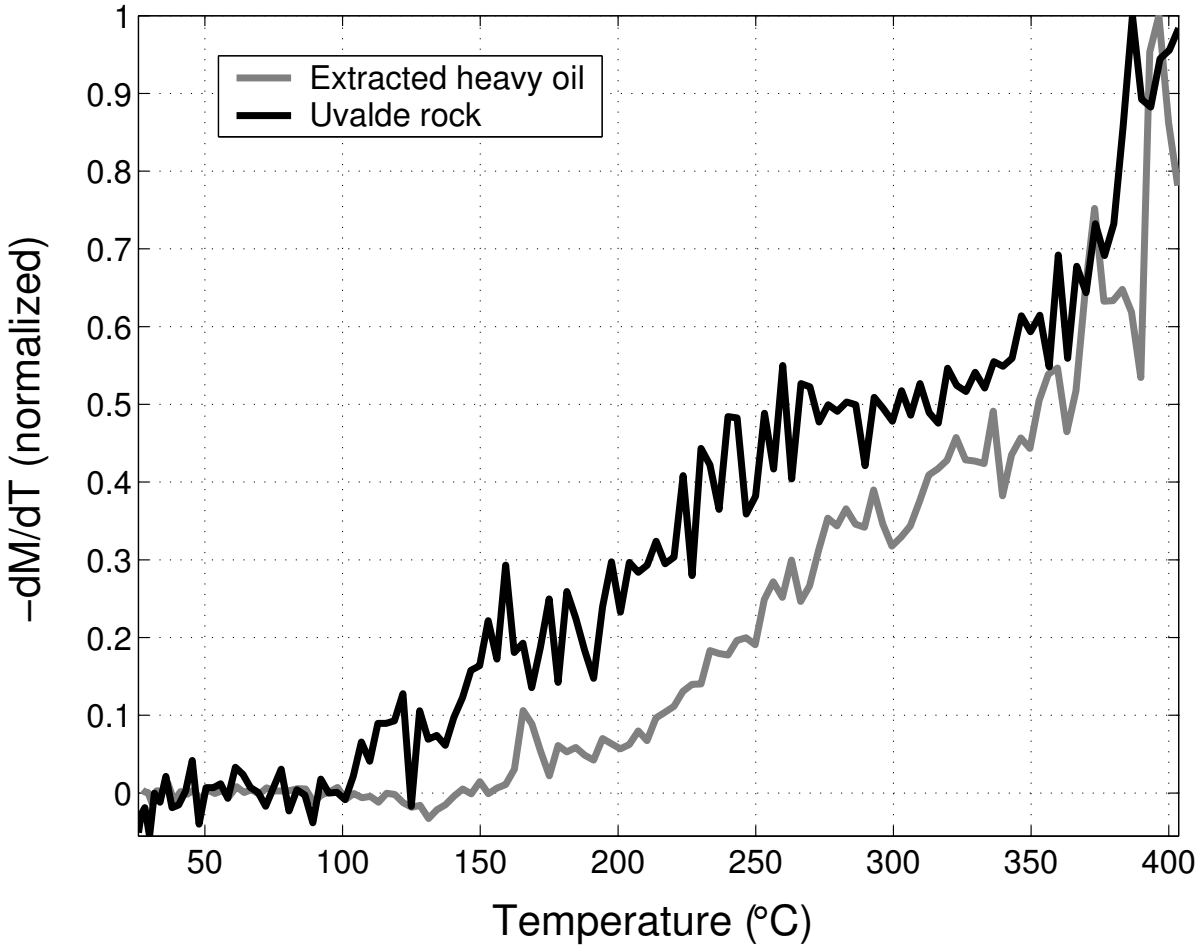

Figure 8. Thermo-gravimetric analysis (TGA) of Uvalde heavy-oil rock (black) and the oil extracted from it (gray).

more efficient transfer of mechanical energy between the molecules/chains. Also at low frequencies, the material has sufficient time to relax almost completely as the molecules/chains slide past each other, which minimizes the energy loss (high Q). The "locking" of the molecules/chains at higher frequencies translates to a high value of Q, as more the "locking", less is the frictional loss. For intermediate frequencies, however, the molecules/chains have a maximum slip during a cycle of loading, leading to maximum frictional loss of energy.

The high frictional loss of energy manifests in a relaxation trough or attenuation peak, seen in Figure 5c. We believe this attenuation peak is caused by viscous relaxation of the heavy oil within the rock (Walsh, 1968; Walsh, 1969). As described by O'Connell and Budiansky (1977), this relaxation occurs between the "saturated isolated" (at low frequencies the shear stresses in the fluid relax completely, but no fluid flows out of the pores/cracks) and "glued" cases (at high frequencies the viscosity of the fluid is high and the shear stresses in the fluid do not relax). If Coulomb frictional sliding between crack surfaces and grain boundary contacts is assumed to be the dominant attenuation mechanism, Q should be independent of frequency (Johnston and Toksöz, 1981), but it is not in this case. So, the frequency dependence of Q rules out friction as the dominant attenuation mechanism. One might speculate that "squirt flow" (Mavko and Nur, 1975; O'Connell and Budiansky, 1977; Vo-Thanh, 1990) could also result in such a relaxation peak. The high viscosity of heavy oil at these low temperatures, however, makes "squirting" of these oils unlikely. One way of helping to understand these observations would be to model the response and compute the aspect ratio of the cracks, as suggested and implemented by O'Connell and Budiansky (1977) and Vo-Thanh (1990). Another way of addressing this puzzle is to analyze the dynamic mechanical response of the heavy oil extracted from the rock. If indeed viscous

relaxation is taking place, we should also observe a relaxation peak in the heavy oil at the same temperatures and frequencies as those in the heavy-oil rock; otherwise "squirt flow" might be taking place.

The two relaxations in Figures 5d and Figures 7d are taking place at identical temperatures and frequencies, thereby strongly implying that viscous relaxation of the heavy oil within the rock is responsible for the observed attenuation peak. The shift in the attenuation peak towards lower frequencies with decreasing temperature is because the effect of the decreasing temperature (increases viscosity) is counteracted by the effect of decreasing frequency (decreases viscosity), so as to sustain the viscous relaxation of the oil.

As mentioned earlier, the strong temperature dependence of the mechanical properties of the heavy-oil rock comes from the melting of the heavy oil (glass transition temperature of $\approx$ 30°C of the heavy oil) and its subsequent composition change at high temperatures. The heavy oil, which is glassy at room temperature, starts melting with increase in temperature, thereby sharply decreasing the shear storage modulus and also the quality factor. Low values of Q, approaching 0 (around 70°C), at this relaxation are due to the relative movement of the constituents of the heavy oil at the molecular level. Note that the low Q values near 150°C caused by fluid-like behavior of heavy oil i.e. it behaves as a Newtonian fluid at these temperatures. The rise in G' and Q for temperatures exceeding 150°C is probably caused by to a compositional change in the heavy oil, wherein the lighter components are lost leaving the heavier asphaltenes behind (Lesueur and Gerard, 1996; Deshpande et al., 2003). Asphaltenes are essentially solid particles (Lesueur and Gerard, 1996) that increase the modulus and Q of the oil. This compositional change can be corroborated from thermogravimetric analysis (Figure 8), which shows the mass of the heavy oil decreasing with increasing temperature. A significant drop in mass at $\approx$ 150°C corresponds to the loss of the lighter components, thereby making the heavy oil stiffer and less attenuative.

The G' for the oil, however, is lower than the rock moduli (Figure 6) because the solid grains making up the rock matrix are stiffer than the oil. The change in G' with temperature for the rock is smaller than that for the oil because the solid rock frame supports shear at all temperatures. The high G' of the rock relative to that of the oil (difference of a few orders in magnitude) at these high temperatures (greater than 150°C), makes the contribution of the oil modulus negligible. At these high temperatures, the negligible dispersion suggests that friction might be the dominant attenuation mechanism. Other mechanisms, however, such as squirt flow and viscous losses in the oil, cannot be ruled out.

2.4 Modeling

In practice, velocity measurements do not exist for all temperatures and frequencies. This necessitates the use of modeling to provide us with the missing data. Laboratory data can be used to establish the right model. Modeling has another advantage, as it can help in uncertainty analysis.

After extensive analysis, we found that Cole-Cole modeling (Cole and Cole, 1941) provides a good fit to the observed data. According to this model, the dynamic complex shear modulus, $\tilde{G}(\omega)$, is given by,

$$\tilde{G}(\omega) = G_\infty - \frac{G_\infty - G_0}{1 + (i\omega/\omega_r)^\alpha}, \quad (17)$$

where, G_0 and G_∞ are the shear moduli at zero and infinity frequencies, respectively. ω_r is the relaxation frequency or the frequency at which the attenuation peak is observed and is given by

$$\omega_r = \frac{G_\infty - G_0}{\eta}, \quad (18)$$

where, η is the viscosity. As observed by Gautam et al. (2003), the complex composition of heavy oils might result in smearing of the relaxation peak, which is controlled by the parameter α.

The result from Cole-Cole modeling of heavy-oil rock at 70°C is shown in Figure 9 along with their 95% confidence intervals. The procedure for computation of the confidence intervals is shown in appendix A. Note the good match between the data and the model. Usually, the modeling parameters are all assumed as real numbers, but our analysis shows that if these parameters are allowed to be complex, the fitting is even better, as seen in Figure 10. Complex G_0, G_∞, and η imply that all the elements in the Cole-Cole model are viscoelastic.

Modeling also helps in comparing the velocity data collected in the laboratory to the velocity observed in the field. Shear-wave velocities were computed from the P-wave velocities given in Schmitt (1999) by assuming a constant (with frequency) Poisson's ratio of 0.16. The two velocities, one computed from a VSP measurement (100 Hz) and the other a sonic log measurement (10 KHz), are shown in Figures 9d and 10d. There is a good match between my laboratory measurements and field velocities. This emphasises that our laboratory measurements can potentially be directly applicable in seismic data analysis.

3 OIL SHALE ANALYSIS

We examined two shale samples from Green River Formation, Colorado - one with a low organic content of $\approx$ 5% and another with a high organic content of $\approx$ 30% (Figure 4), again considering the influence of temperature and frequency on the physical properties, modulus and attenuation. We also examined the influ-

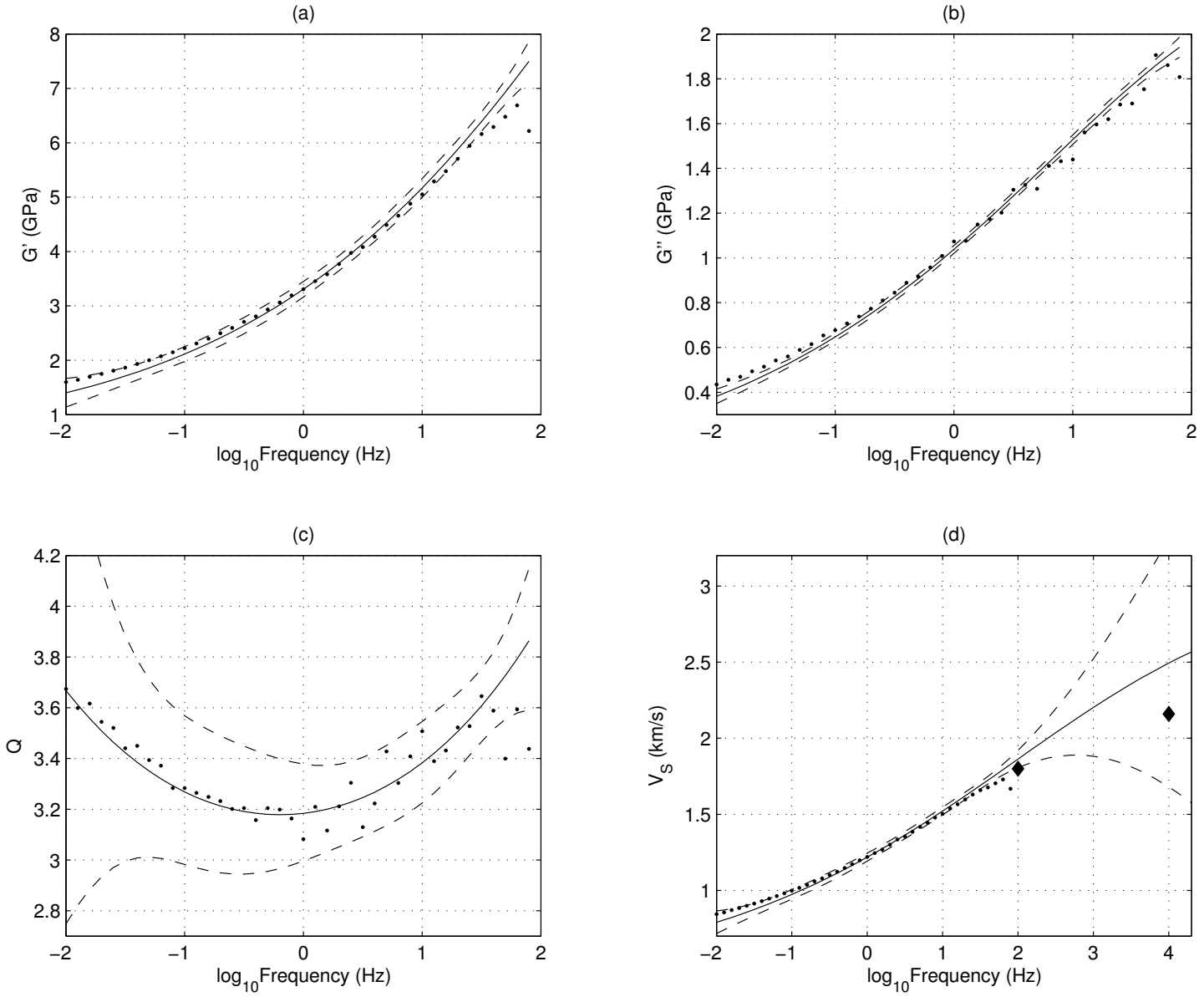

Figure 9: The shear (a) storage modulus (G'), (b) loss modulus (G''), and the (c) quality factor Q, and the (d) shear velocity V_S of the Uvalde heavy-oil rock at 70°C with 95% confidence intervals (shown by dots). The modeled data using Cole-Cole modeling is given by the solid lines. The model parameters are $G_0 = 0.48$ GPa, $G_\infty = 21.48$ GPa, $\eta = 0.0035$ GPa.s, and $\alpha = 0.261$. Velocity data obtained from Schmitt (1999) is shown by the two ♦ in (d).

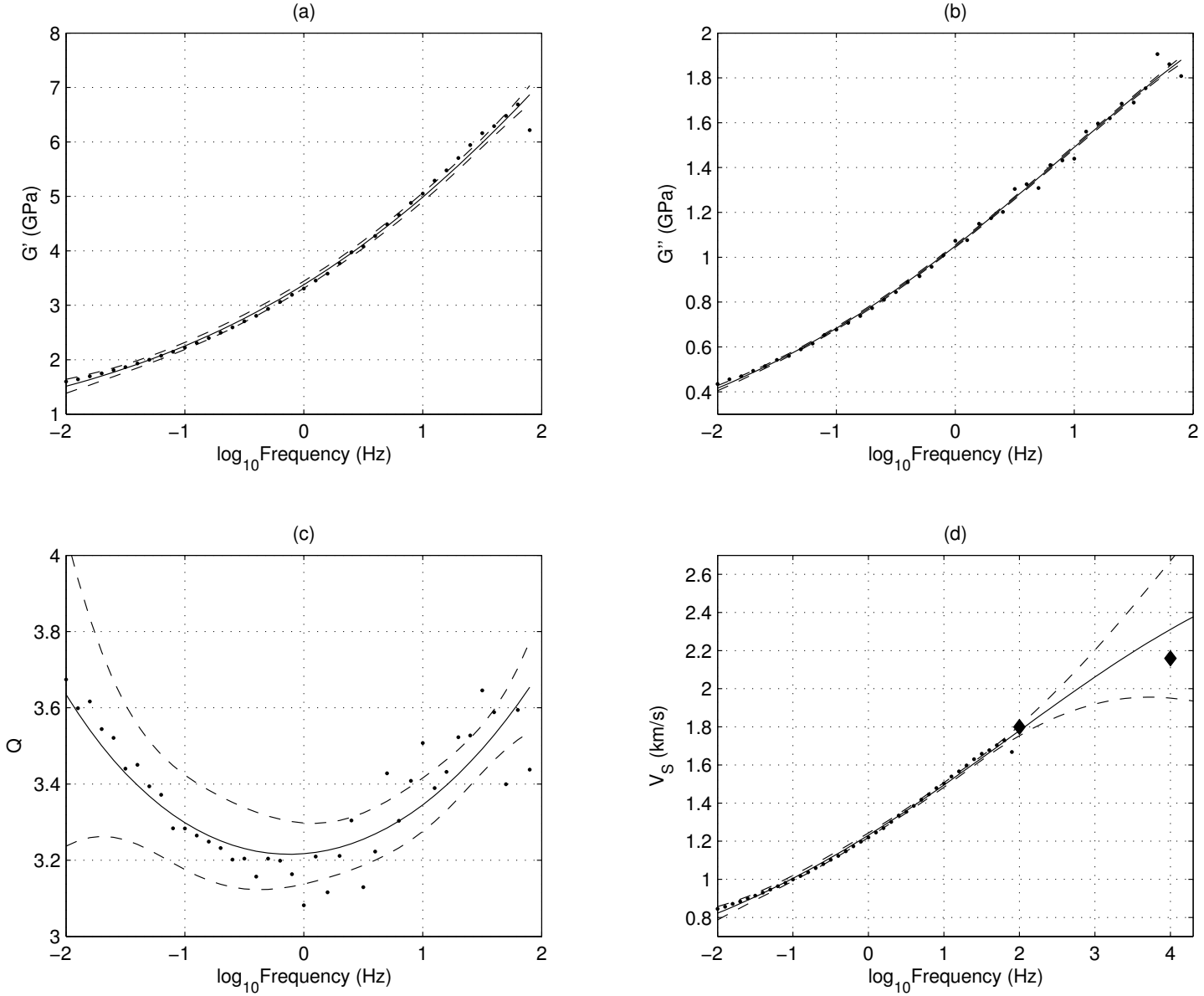

Figure 10: Same as in Figure 9 but with complex model parameters. The model parameters are $G_0 = 0.3 - i0.05$ GPa, $G_\infty = 19.37 + i0.87$ GPa, $\eta = 0.0026 + i0.0004$ GPa.s, and $\alpha = 0.225 + i0.0026$.

ence on shear wave velocity anisotropy and attenuation anisotropy. The anisotropy studies were conducted by using samples cut along three orthogonal planes (Figure 11). We assume the shales to be transversely isotropic (TI), which has been seen in similar shales by many researchers (Vernik and Nur, 1992; Johnston and Christensen, 1995; Vernik and Liu, 1997; Carcione, 2000). A sample cut parallel to the symmetry axis is used to measure the complex stiffness $\tilde{C}_{44} = \tilde{C}_{55}$ (Figure 11). As the shale is TI, a sample cut in the vertical symmetry plane with its long axis orthogonal to the symmetry axis (Figure 11) would give $\tilde{C}_{44} = \tilde{C}_{55}$ as well (Thomsen, 1986; Tsvankin, 2005). In fact, two kerogen-rich samples contained in the vertical symmetry plane, one oriented along the symmetry axis and the other perpendicular to it, gave strikingly similar results for the whole range of temperatures and frequencies studied. This supports our assumption that the shales are very likely TI. A sample cut in the isotropy plane, as shown in Figure 11, is used to obtain $\tilde{C}_{66}$.

3.1 Kerogen-rich shale

Dynamic mechanical analysis of the kerogen-rich shale (Figure 4) is carried out for temperatures ranging from 30°C to 350°C at 20°C increments, with the frequency varying from 0.01 to 80 Hz in increments of 0.1 on the $\log_{10}$ scale. All the measurements are carried out in the linear viscoelastic regime, at a constant strain of $8\text{x}10^{-5}$, under a variable applied axial stress which does not allow the sample to expand vertically. This is similar to reservoir recovery conditions where the shale is heated but its expansion is restricted.

3.1.1 Observations

Figures 12a-b show the real and imaginary components of $\tilde{C}_{55}$, respectively, and Figures 12c and 12d show $1/Q_{55}$ and Q_{55}. Real and imaginary components of $\tilde{C}_{66}$ are shown in Figures 13a and 13b, with $1/Q_{66}$ and Q_{66} in Figures 13c and 13d, respectively.

As seen in Figures 12a and 13a, frequency dispersion is relatively weak in these kerogen-rich shales evident from the small change in C'_{55} and C'_{66} with frequency. Both storage moduli (C'_{55} and C'_{66}) increase with frequency, even though the increase is small with the most noticeable change in the vicinity of 150°C. Attenuation in both directions is also weakly dependent on frequency, with an attenuation peak at $\approx$ 150°C. At higher temperatures, however, attenuation shows a stronger dependence on frequency, where it decreases with frequency.

Both moduli (C'_{55} and C'_{66}) and quality factors (Q_{55} and Q_{66}) show a marked change with temperature (also observed on common inorganic shales by Johnston, 1987). Figure 14 shows a comparison of the moduli and attenuation data (along the two directions) for 0.3 Hz. C'_{55} and C'_{66} both drop sharply with increasing temperature up to $\approx$ 200°C. The drop in C'_{55} is greater than that in C'_{66}. With increase in temperature, C'_{55} rises, reaches a maximum, and then drops again. In contrast, C'_{66} shows relatively little change for temperatures greater than $\approx$ 200°C, but drops again at higher temperatures. Both Q_{55} and Q_{66} show similar behavior with temperature. They drop from $\approx$ 40 at room temperature to below 5 at $\approx$ 150°C, increase with further increase in temperature, and then a small drop at $\approx$ 300°C.

The difference in moduli and attenuation along the two directions can be conveniently represented using Thomsen's SH velocity anisotropy parameter γ (Thomsen, 1986) and the SH-wave attenuation anisotropy parameter γ_Q defined by Zhu and Tsvankin (2006) as the fractional difference between the attenuation coefficients in directions orthogonal and parallel to the symmetry axis:

$$\gamma_Q = \frac{Q_{55} - Q_{66}}{Q_{66}}. \tag{19}$$

γ and γ_Q for the whole frequency and temperature range are shown in Figures 15a and 15b, respectively. SH velocity anisotropy can be significantly strong, attaining values as high as 3; attenuation anisotropy can also be significant, with values nearing 2. In laboratory and field conditions, γ has been found to be less than 0.5, which is significantly lower than the maximum value of γ observed by us. Note that the sign of γ_Q can change. The weak frequency dependence of $\tilde{C}_{55}$ and $\tilde{C}_{66}$ translates to a generally weak dependence of γ and γ_Q on frequency. γ_Q, however, shows a moderately strong dependence on frequency at high temperatures. Temperature, on the other hand, has a marked effect on γ and γ_Q. To illustrate this better, we plot γ and γ_Q for a particular frequency (0.3 Hz) in Figures 14a and 14b, respectively. γ rises sharply (from a value of $\approx$ 0.2, which matches with the value measured by Mah, 2005) with increasing temperature, peaking at $\approx$ 180°C to a value of 2.5; it decreases thereafter till about $\approx$ 290°C, after which it rises again. γ_Q shows a trend opposite that of γ; also the change in γ_Q is not as prominent as in γ.

3.1.2 Mechanisms

At low frequencies, the shales have time to undergo deformation (relaxed state), which reduces the storage modulus, while with increasing frequency, the time available for the particles to move decreases, making the shale stiffer. Within the seismic bandwidth dispersion is essentially absent.

In this case the observed attenuation likely is predominantly caused by frictional dissipation owing to relative motions at grain boundaries (Walsh, 1966), or at interfaces between mineral and kerogen surfaces. The rapid drop in C'_{55} and the relatively smaller drop in C''_{66} at $\approx$ 120°C is probably due to the liquefaction of the

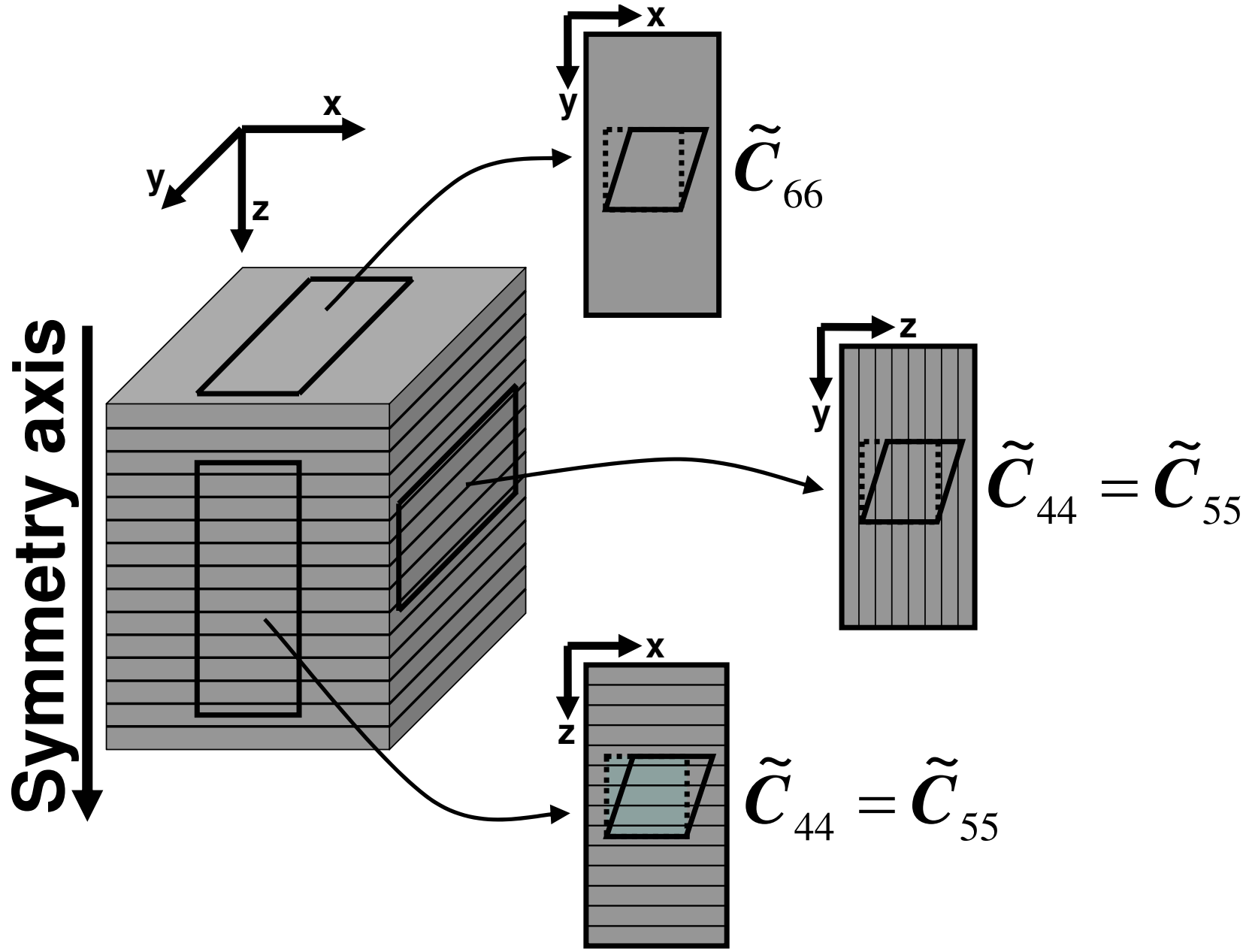

Figure 11: Shale samples cut in specific directions to compute $\tilde{C}_{44} = \tilde{C}_{55}$ and $\tilde{C}_{66}$.

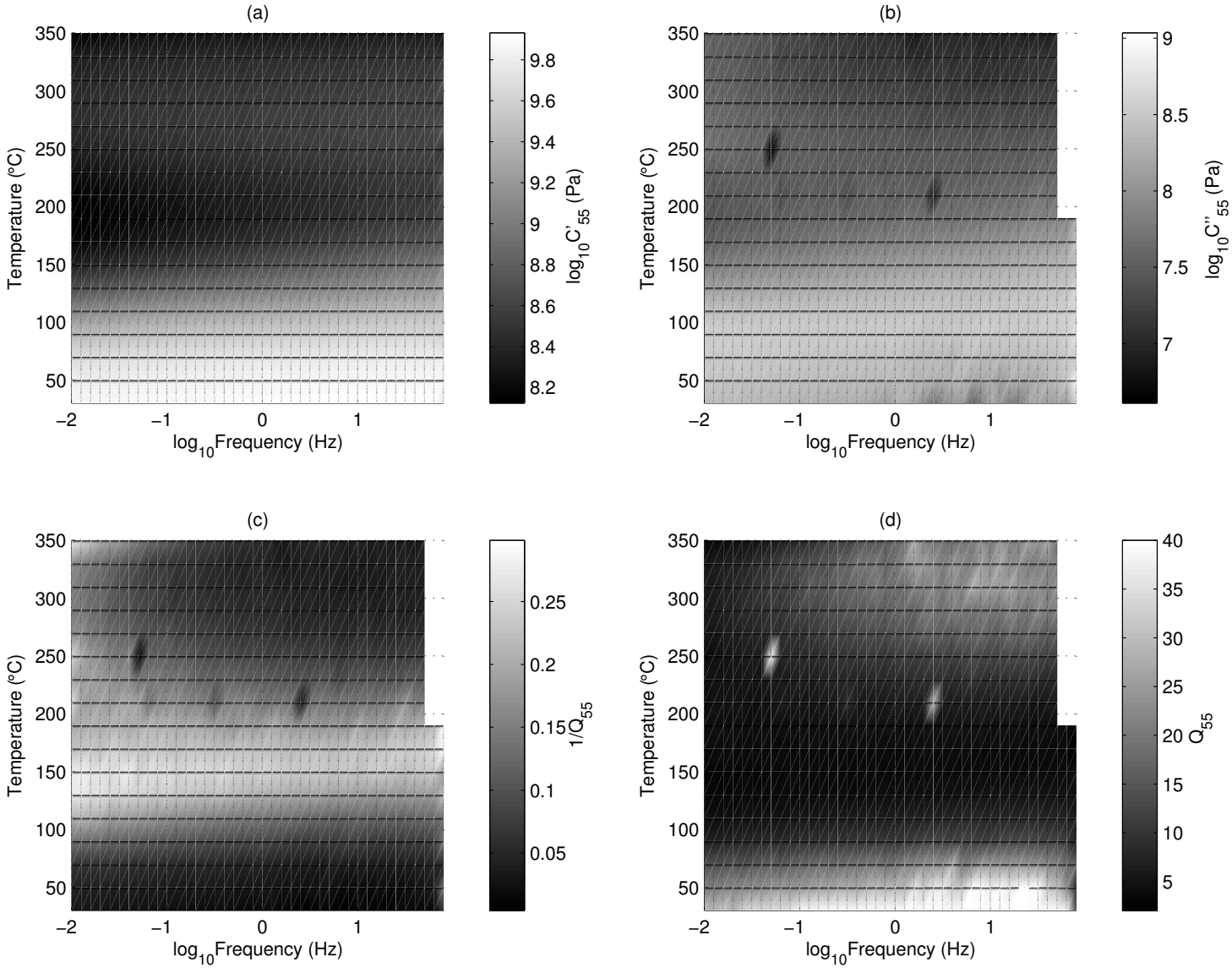

Figure 12: The shear (a) storage modulus (C'_{55}), (b) loss modulus (C''_{55}), (c) $1/Q_{55}$, and the (d) quality factor Q_{55} (in modified color scale) of the kerogen-rich shale.

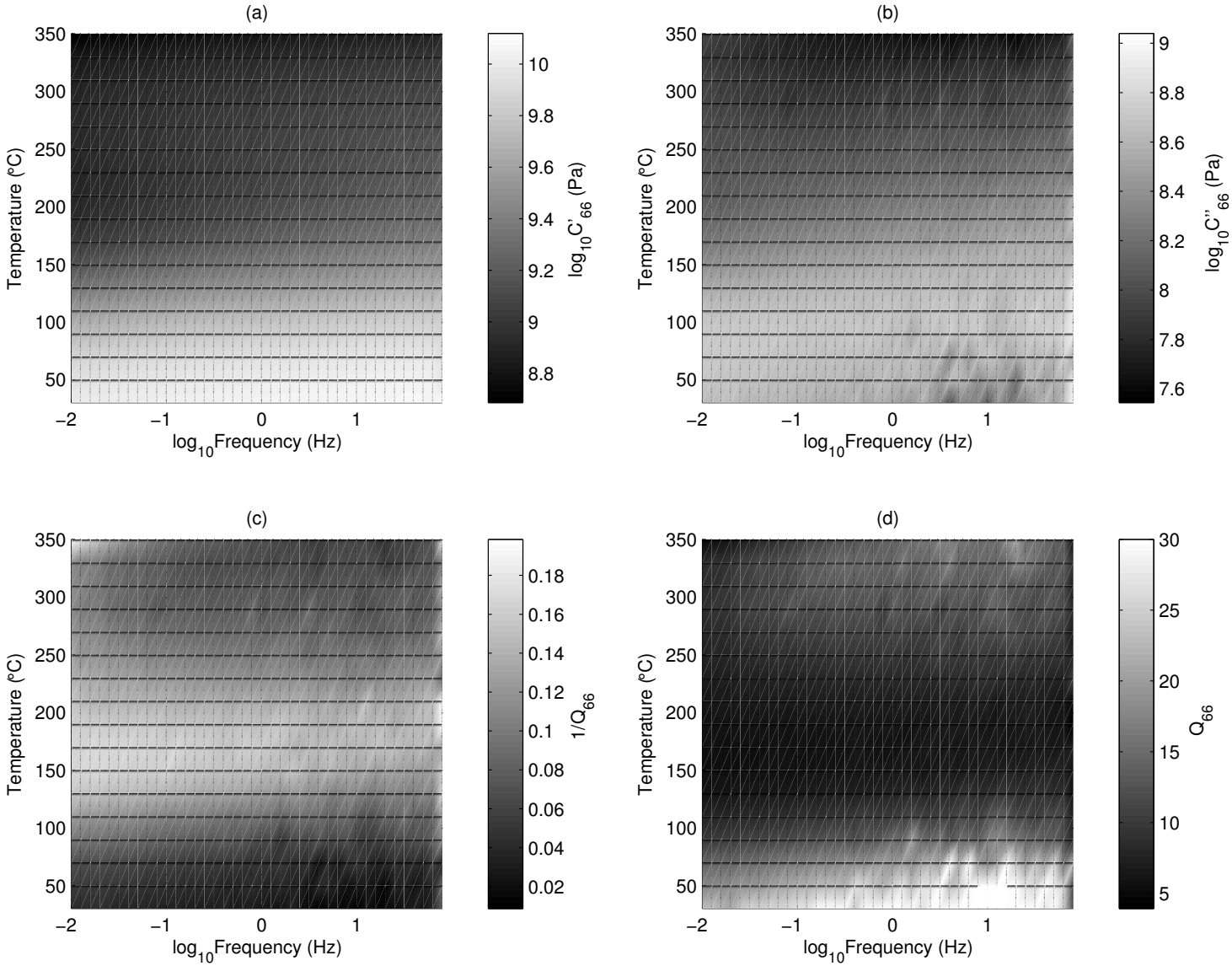

Figure 13: The shear (a) storage modulus (C'_{66}), (b) loss modulus (C''_{66}), (c) $1/Q_{66}$, and the (d) quality factor Q_{66} of the kerogen-rich shale. The color scale in (d) is modified to show the trends for Q_{66}.

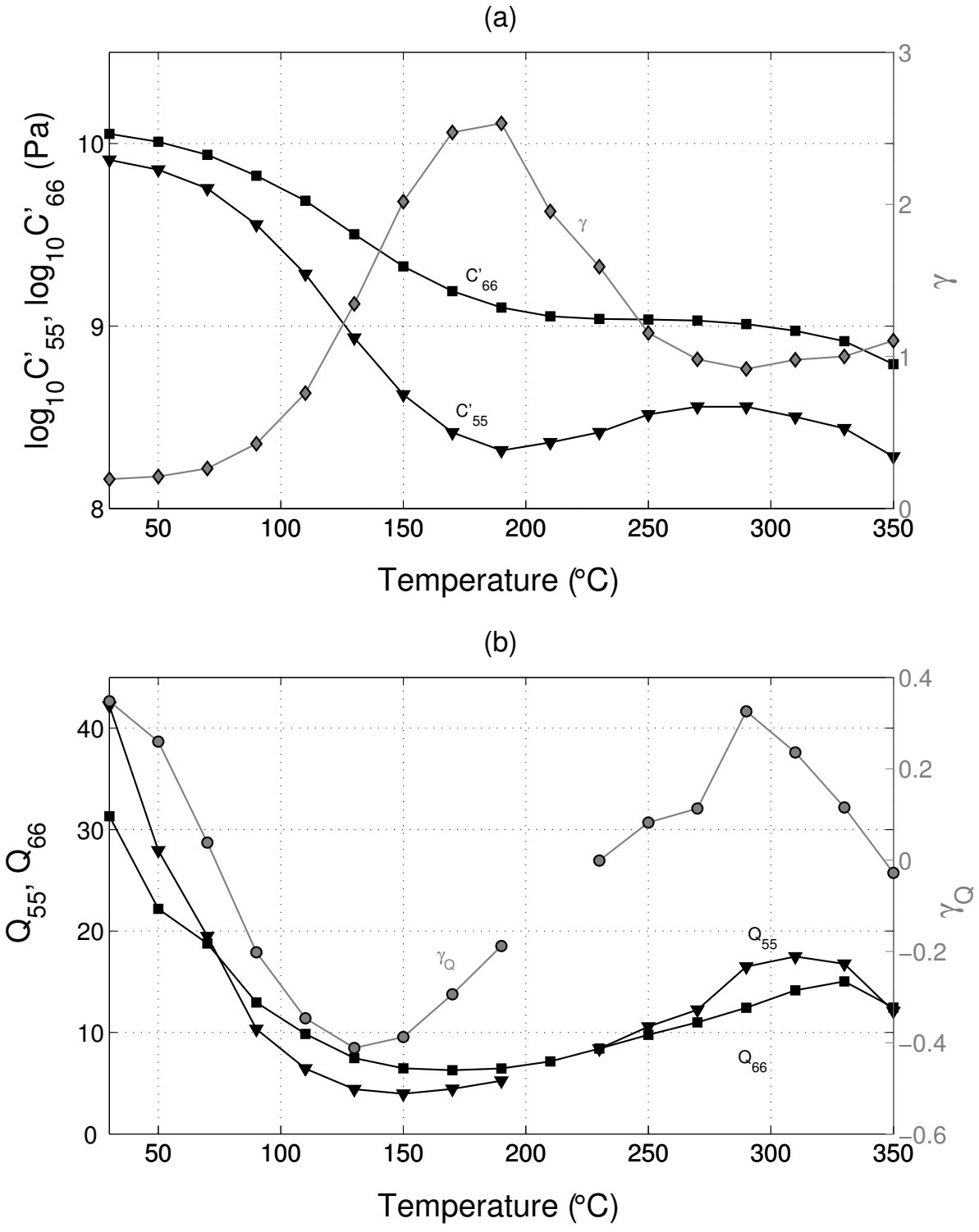

Figure 14. (a) C'_{55} (triangles), C'_{66} (squares) and γ (diamonds) (b) Q_{55} (triangles), Q_{66} (squares) and γ_Q (circles) of the kerogen-rich shale at a frequency of 0.3 Hz.

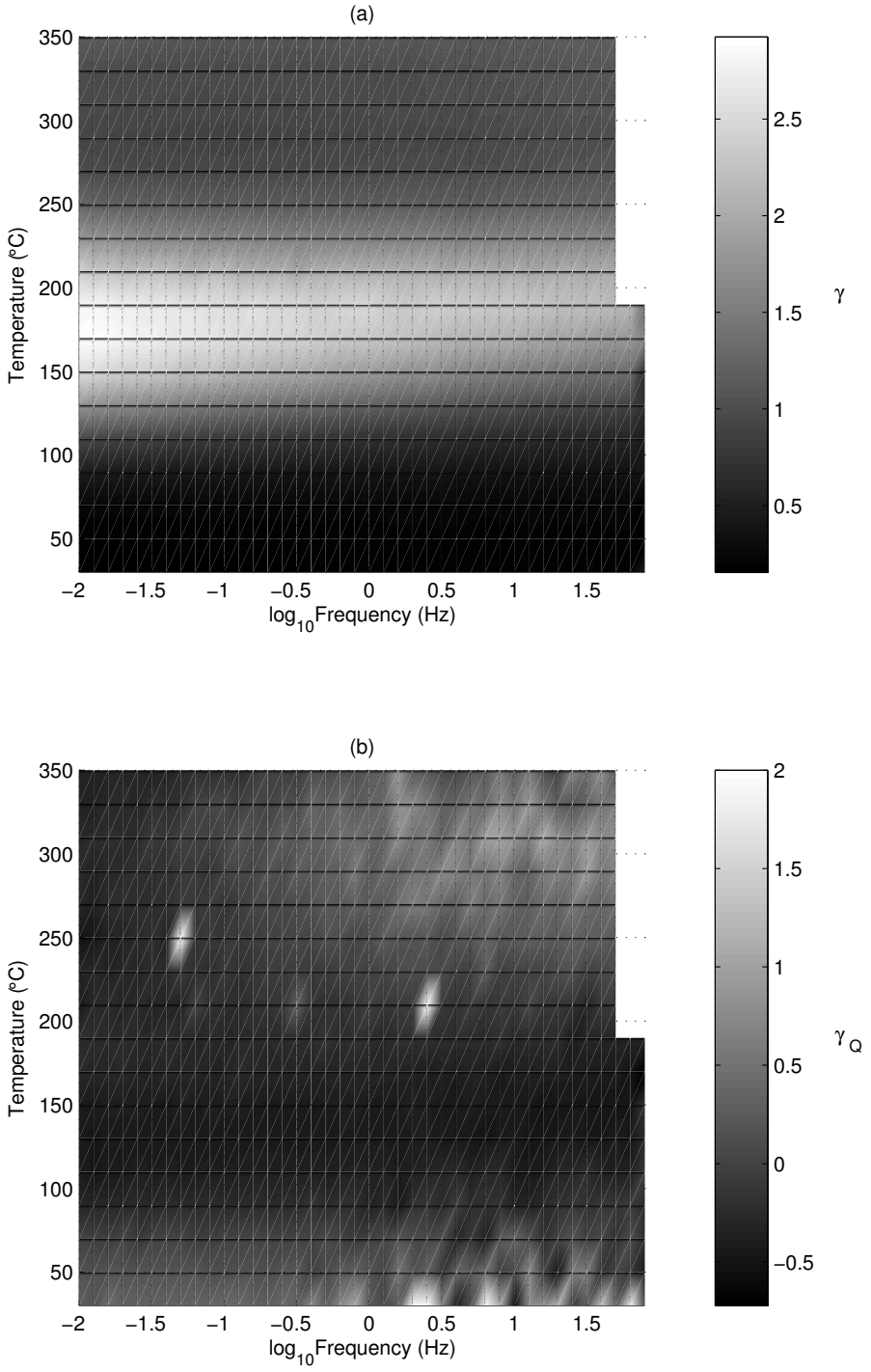

Figure 15. The SH-wave (a) velocity anisotropy paramater γ, and (b) attenuation anisotropy parameter γ_Q in the kerogen-rich shale.

kerogen in the shale. Carcione (2000) suggested that $\tilde{C}_{55}$ is mostly controlled by the isotropic kerogen in the shales while $\tilde{C}_{66}$ is dominated by the clay in the layering. With temperature increase, the kerogen in the shale melts, which in turn facilitates relative sliding between the clay layers. The shale thus becomes softer and more lossy as a result of increased frictional sliding. This lowers the quality factor, as seen in Figures 12d and 13d. Both Q_{55} and Q_{66} show a negligible dependence on frequency, perhaps an indication of a broad relaxation mechanism. Whether it is attributable to viscous relaxation of the fluid or to "squirting" of the fluid in the cracks can possibly be determined by computing the crack aspect ratio, as suggested by O'Connell and Budiansky (1977). With further increase in temperature, the kerogen is altered and partially expelled, thereby increasing the stiffness and decreasing any frictional losses as well, as evident from the increase in Q, as seen in Figures 12d and 13d.

It is common knowledge that shales are anisotropic. Wave propagation in a particular direction depends on the medium properties seen by the particle motion induced by the wave. A change in the weak layers in the shale have a greater influence on the bedding-perpendicular direction than on the bedding parallel direction. Thus, any change to the zones of weaknesses (kerogen layers) would affect $\tilde{C}_{55}$ much more than $\tilde{C}_{66}$. This can be seen by comparing Figures 12 and 13, where $\tilde{C}_{55}$ shows a much more rapid change than does $\tilde{C}_{66}$, caused by melting and evaporation of the kerogen.

It is especially convenient to analyze the anisotropy parameters (γ and γ_Q). As the kerogen melts, C'_{55} drops significantly compared to C'_{66}, resulting in a jump in γ. With further increase in temperature, kerogen starts evaporating, which results in a drop in γ as the shale becomes less compliant, thus increasing C'_{55} but not C'_{66} (Figure 14a). Note that the velocity anisotropy parameter, γ, changes by a factor of 10 (Figure 15a) which is significant and could be detectable in 4D-studies. The initial drop in γ_Q (Figure 15b) is due to the rapid drop in Q_{55}. Subsequently, as the kerogen starts evaporating, Q_{55} also increases, resulting in an increase in γ_Q. As with velocity anisotropy, attenuation anisotropy also shows a large change with temperature, which again could dramatically change seismic signatures.

This experiment also shows the contribution of layering to the anisotropy of TI media. Bakulin (2003) has shown that the effect of layering on VTI anisotropy is of second order compared to that of intrinsic anisotropy, but if the contrast in moduli between the different layers is large, the layer-induced anisotropy can be significant. At room temperatures, the kerogen is solid and so the contrast in shear modulus of the solid clay (and carbonate) layers and the kerogen layers is not significant. This results in a low value of γ at room temperatures (Figure 15a). With increase in temperature, the kerogen progressively melts, thereby increasing the contrast between the layers. This results in a notable increase in γ caused by layering.

3.2 Lean shale

We also analyzed shales with 5% organic content at the same temperatures and frequencies as those for the kerogen-rich shales. Again all measurements are done in the linear viscoelastic range and under a confining axial stress. These lean shales are gray colored because of the lack of kerogen in contrast to the kerogen-rich shales, which are brownish-black (Figure 4).

3.2.1 Observations and mechanisms

The $\tilde{C}_{55}$ component of the lean shale is shown in Figure 16, while $\tilde{C}_{66}$ is given in Figure 17. The general trends for lean shale are similar to those for the kerogen-rich shale. The magnitudes of lean-shale moduli, however, are larger than those of the organic-rich shales.

Frequency dispersion is weak (Figures 16a and 17a). The small increase in both moduli (C'_{55} and C'_{66}) is not significant, especially within the seismic band. Attenuation is also weakly dependent on frequency (Figure 16d). Q_{66} (Figure 17d) looks very noisy, so we could not derive any firm conclusions. As for the kerogen-rich shales, attenuation shows a stronger dependence on frequency at high temperatures than at low temperatures. This weak frequency dependence at intermediate temperatures (around 150°C) of attenuation implies that friction may be the dominant attenuation mechanism. Later, we will give more evidence in favor of frictional attenuation. Additional experiments, however, are necessary to find out if other mechanisms, such as "squirt flow" of fluids and viscous relaxation, are playing important roles.

With increase in temperature, till about 200°C, C'_{55} drops more rapidly than does C'_{66}. This fall in the storage moduli is most probably due to the liquefaction of the small amount of kerogen sandwiched between the clay layers. As discussed earlier in the previous section, any change to the kerogen would influence $\tilde{C}_{55}$ much more than $\tilde{C}_{66}$, which explains the greater drop in C'_{55}. Below 200°C, the liquefaction of kerogen not only softens the rock, bringing down C'_{55}, but also decreases the quality factor, Q_{55}, sharply, as seen in Figure 16d. This is because the liquid kerogen facilitates sliding, thereby decreasing the efficiency of transfer of mechanical energy between clay particles and increasing frictional loss.

With further heating, the lighter components of the kerogen evaporate, making the shale stiffer. Again, only $\tilde{C}_{55}$ is expected to be influenced and not $\tilde{C}_{66}$, which can be seen in Figures 16 and 17. The quality factor Q_{55} also increases as the frictional sliding between the clay layers is reduced.

To test if friction is the dominant loss mechanism, we conducted another set of measurements to find C'_{55}

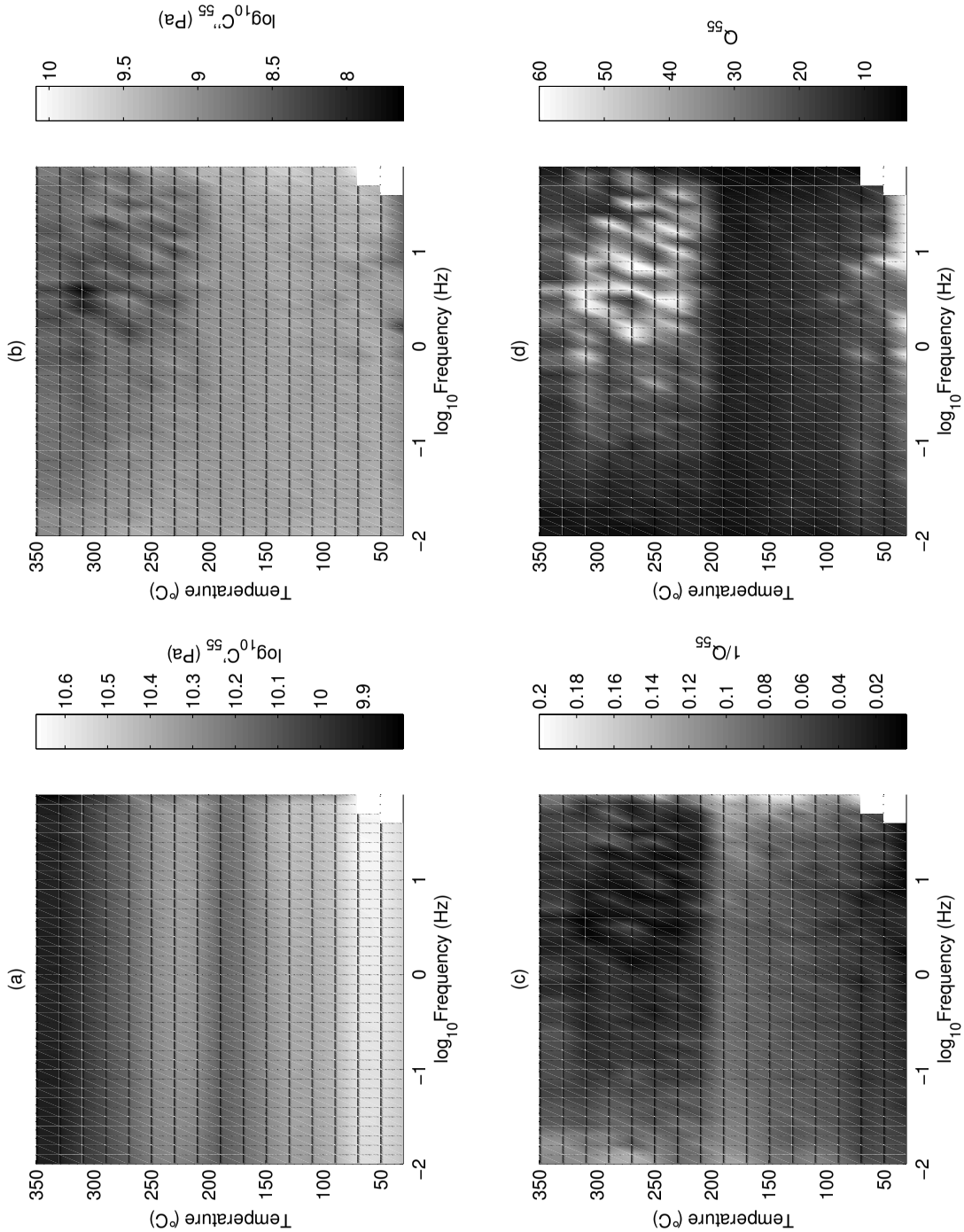

Figure 16: The shear (a) storage modulus (C'_{55}), (b) loss modulus (C''_{55}), (c) $1/Q_{55}$, and (d) quality factor Q_{55} of the lean shale.

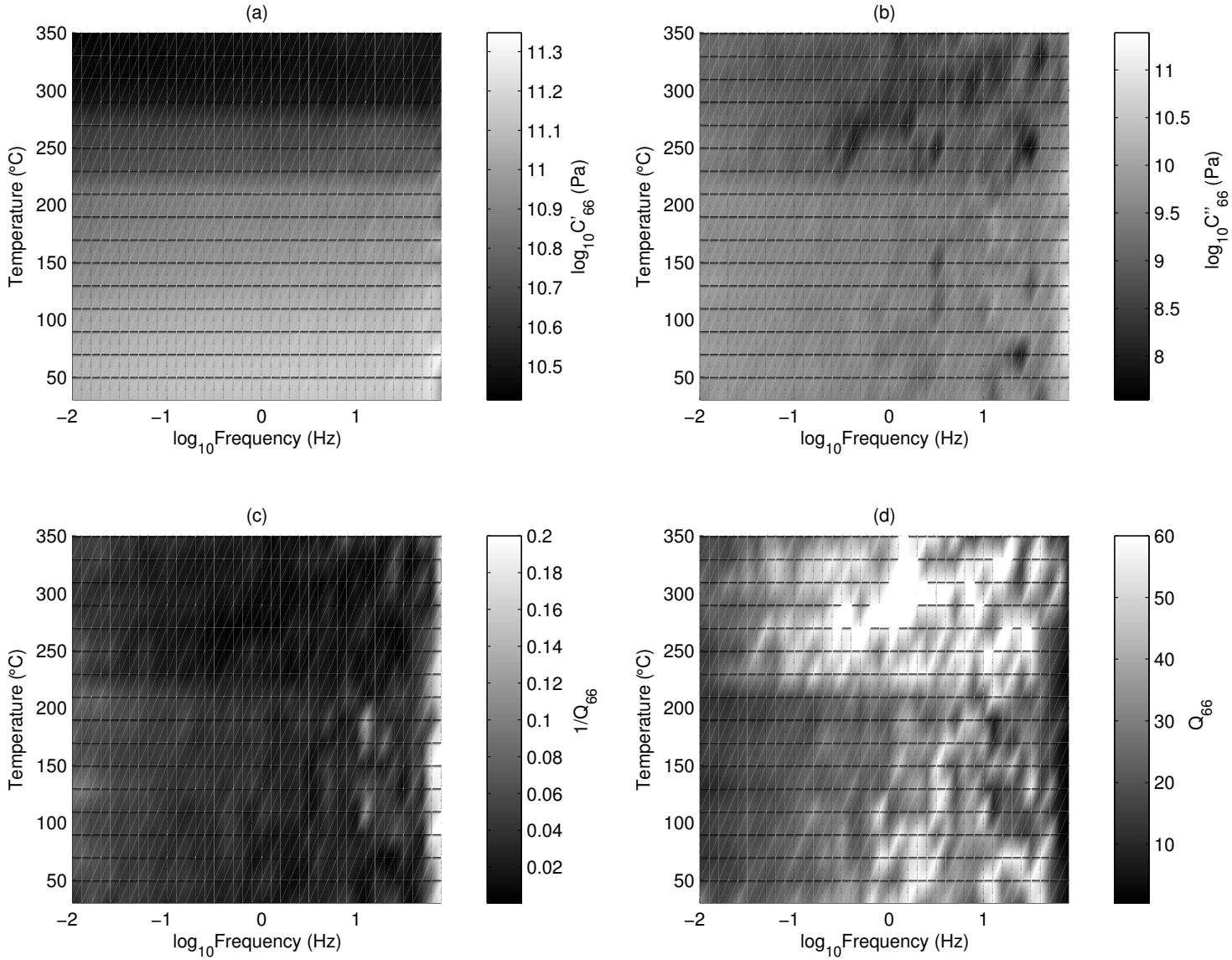

Figure 17: The shear (a) storage modulus (C'_{66}), (b) loss modulus (C''_{66}), (c) $1/Q_{66}$, and the (d) quality factor Q_{66} of the lean shale.

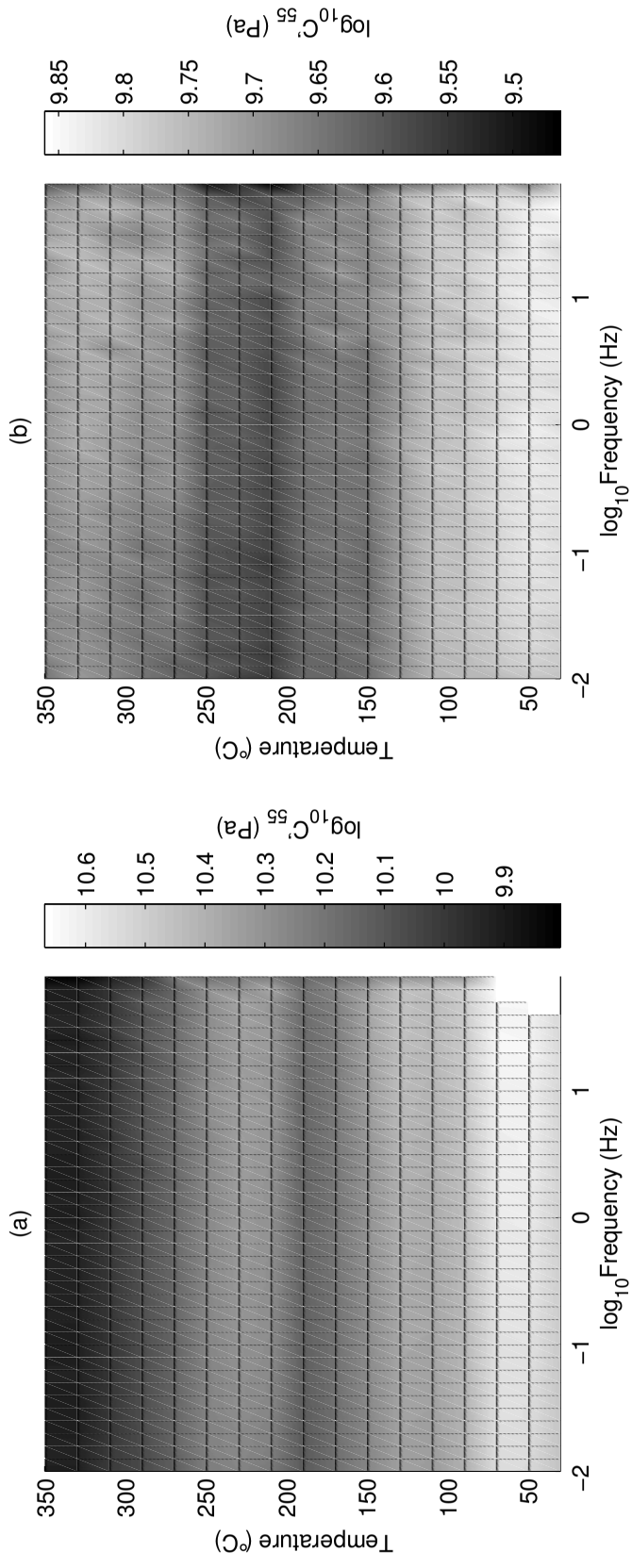

Figure 18: C'_{55} of the lean shale measured under (a) confining axial stress (same as Figure 16a) and (b) constant axial stress.

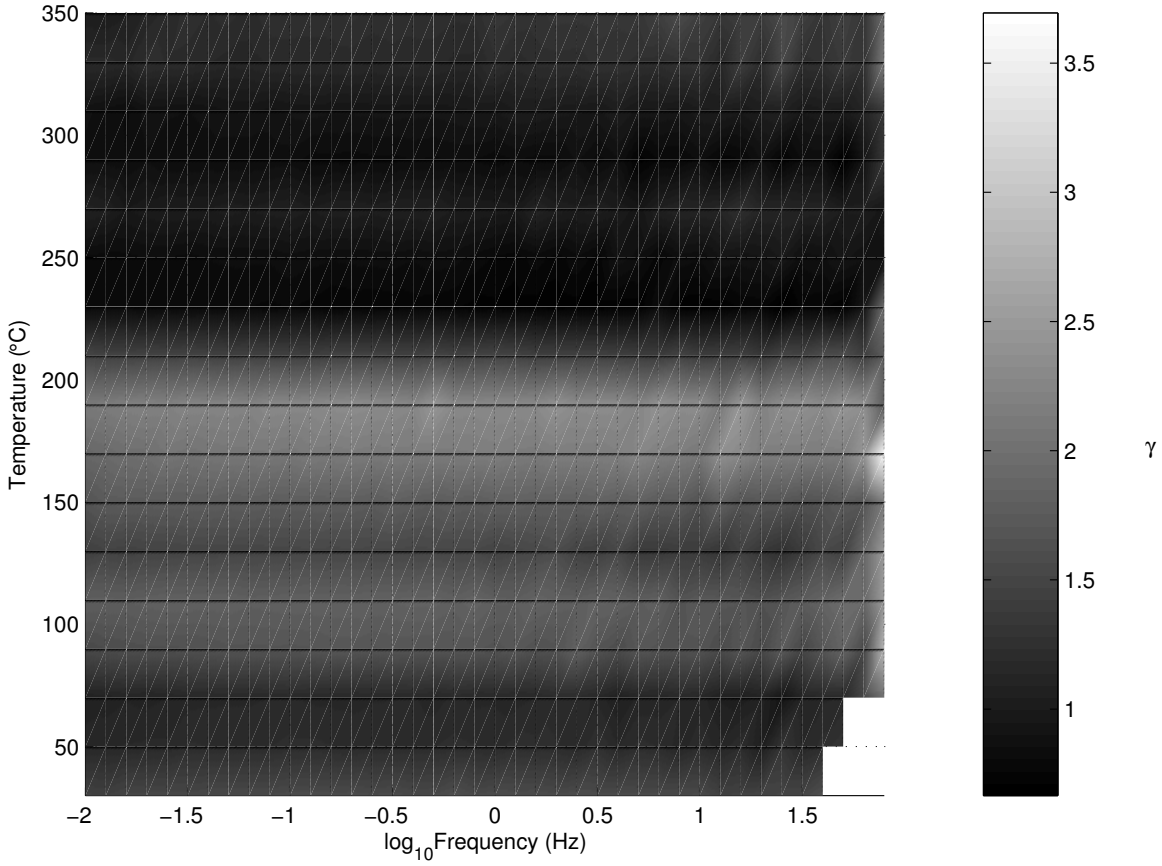

Figure 19. The SH-wave velocity anisotropy parameter γ of the lean shale.

under constant axial stress, results for which are shown in Figure 18b. If friction were indeed the dominant loss mechanism, two major changes would occur. First, C'_{55} would decrease in general. Second, for temperatures above 200°C, just as when the kerogen is lost, C'_{55} under constant axial stress would continue to decrease. This is because under constant axial stress, after loss of some kerogen, the voids left behind are retained, which decreases C'_{55} further. In contrast, under increasing axial stress, the voids are occupied by the expanding clay minerals as the rock is not allowed to expand. Both these effects can be seen by comparing Figures 18a and 18b, which support friction as the dominant attenuation mechanism.

The effect of melting of kerogen and its subsequent evaporation can be better seen by analyzing the anisotropy parameter γ, shown in Figure 19. With melting of kerogen, γ increases as the difference between the two stiffnesses (C'_{55} and C'_{66}) increases. Above 200°C, γ drops because of the loss of some kerogen from the shale.

4 DISCUSSION AND CONCLUSIONS

Unlike common fliuds (e.g. brine and light oil), heavy oils and kerogens found in heavy-oil rocks and oil shales, respectively, act as solids at room temperatures and fluids at higher temperatures. In other words, at room temperature, heavy oils and kerogens support a shear wave, but not at higher temperatures where the shear modulus approaches zero. They would, however, have a non-zero bulk modulus at all temperatures and the percentage change in the bulk modulus would smaller compared to the change in shear properties. So the shear study of these rocks is more attractive than the study of their bulk properties and thus makes acquisition of multicomponent seismic data all the more important. Our shear wave measurements, as a function of temperature,

should be representative of the conditions encountered during in-situ steamflooding of heavy oil reservoirs and thermal cracking and steamflooding of oil shale reservoirs. Moreover, as heavy-oil rocks and oil shales are effectively viscoelastic, their properties in the seismic band would be significantly different from that in the logging-frequency range and the ultrasonic band. The shear properties, acquired at frequencies ranging from 0.01 to 80 Hz (which includes the seismic band), should be close to the seismic properties of heavy oils and oil shales in the field.

The negligible frequency dependence of the moduli and attenuation within the seismic bandwidth, both for the heavy oils and oil shales, makes exploitation of frequency-dependent analysis unlikely. For heavy oils, however, there could be significant differences in properties between seismic, log, and ultrasonic frequencies. Most of the existing methods for Q estimation from field data assume a constant Q within the seismic bandwidth, a resonable approximation as shown by our laboratory measurements.

The strong temperature dependence of the mechanical properties of heavy oils and oil shales makes 4D-9C seismic analysis promising. Temperature has a dramatic influence on velocity as well as on attenuation, and thus on traveltimes and amplitudes of shear waves. For example, on heating a heavy oil reservoir, the shear-wave velocity might decrease by a factor of 3, while the quality factor can decrease by a factor of 10. Seismic data can be exploited to estimate the physical state of the rock, thus the local temperature. As has already been used in many studies, the direction and extent of the steam front can also be detected from seismic data.

Like heavy-oil rocks, oils shales show a strong dependence of modulus and attenuation on temperature. The melting of kerogen can bring down the shear velocity significantly, by as high as five times in some cases. Their quality factor can also drop by a factor of 10 when going from room temperature conditions to $\approx 150^{\circ}$C. So reservoir areas affected by heat should show a noticeable drop in velocities accompanies by significant increase in attenuation.

Oil shales have an additional property to be exploited - anisotropy. The fact that temperature influence on C'_{55} and C'_{66} are differs, makes anisotropy an important propetry. We have seen how dramatic the effect of temperature on both velocity anisotropy (γ) and attenuation anisotropy (γ_Q) can be. Such large changes in anisotropy could be visible in seismic data. For example, there should be a notable change in the nonhyperbolic moveout of SS-waves. Our measurements are also serve the purpose of studying the contribution of layering to the anisotropy of shales, where the melting kerogen increases the contrast in properties between the layers, thereby increasing the anisotropy. Thus the heat-affected zones in the oil shale reservoir should show higher anisotropy than the unaffected part. The original kerogen content in a shale also influences the behavior of the shale with temperature. From our study, we see that lean-shales have higher storage moduli and higher Q than more organic rich shales. Also the change in velocity anisotropy and attenuation anisotropy is greater in shales richer in organic content. This can potentially be used to estimate the organic content of shales.

Thus, our whole suite of measurements should be directly applicable in seismic analysis of heavy oil and oil shale reservoirs during their exploration, development and production. The high sensitivity of shear waves to temperature effects on these reservoirs, makes acquisition of multicomponent seismic data important.

5 RECOMMENDATIONS

We have studied heavy oils and oil shales under different temperature conditions. It is also important to understand their behavior with varying pressure. Moreover, torsional experiments yield only shear properties of the materials. But the majority of the existing data is P-wave data, which with already existing processing procedures, is also better understood than are S-waves. It is, therefore, important to study the P-wave properties for heavy oils and oil shales within the seismic bandwidth. Anisotropy, both P-wave and S-wave, of oil shales needs more attention, because of the large sensitivity of shales to temperature changes. Additional work needs to be carried out to test the dependence of all the above physical properties on strain amplitude.

6 ACKNOWLEDGEMENTS

We thank Dr. John Dorgan of Chemical Engineering at CSM for allowing us to use his laboratory facilities. We appreciate Prof. Ken larner's help in editing this manuscript, and also the help of Prof. Luis Tenorio on statistical analysis of the data. We are grateful to the sponsors of Center for Wave Phenomena and Center for Rock Abuse for their financial support. We would also like to thank Xiaoxia Xu, Manika Prasad, and Rodrigo Fuck, for many animated yet fruitful discussions.

REFERENCES

Bakulin, A., 2003, Intrinsic and layer-induced VTI anisotropy: 73rd Annual International Meeting, SEG, Expanded Abstracts.

Batzle, M., B. Zadler, R. Hofmann, and D. Han, 2004, Heavy oils Seismic properties: 74th Annual International Meeting, SEG, Expanded Abstracts.

Batzle, M., R. Hofmann, M. Prasad, G. Kumar, L. Duranti, and D. Han, 2005, Seismic attenuation: Observations and mechanisms: 75th Annual International Meeting, SEG, Expanded Abstracts.

Carcione, J. M., 2000, A model for seismic velocity and attenuation in petroleum source rocks: Geophysics, **65**, 1080–1092.

Cole, K. S., and R. H. Cole, 1941, Dispersion and absorption in dielectrics-I, alternatinf current characteristics: J. Chem. Phys., **9**, 341-351.

Curtis, C., R. Kopper, E. Decoster, A. G. Garcia, C. Huggins, L. Knauer, M. Minner, N. Kupsch, L. M. Linares, H. Rough, and M. Waite, 2002, Heavy-oil reservoirs: Oilfield Review, **14**, 30–51.

Deshpande, A. P., S. Varughese, A. Shahanawaz, and M. V. Arun, 2003, Microstructure-related rheological behaviour of asphalt: IIT-Madras, Chennai.

Futterman, W. I., 1962, Dispersive body waves: J. Geophysical Res., **67**, 5279–5291.

Gallant, A. R., 1987, Nonlinear statistical models: Wiley, New York.

Gautam, K., M. Batzle, and R. Hofmann, 2003, Effects of fluids on attenuation of elastic waves: 73rd Annual International Meeting, SEG, Expanded Abstracts.

Han, D., J. Liu, and M. Batzle, 2005, Measurement of shear wave velocity of heavy oil: 75th Annual International Meeting, SEG, Expanded Abstracts.

Hedlin, K., L. Mewhort, and G. Margrave, 2001, Delineation of steam flood using seismic attenuation: 71st Annual International Meeting, SEG, Expanded Abstracts.

Iwasaki, T., F. Tatsuoka, and Y. Takagi, 1978, Shear moduli of sand under cyclic torsional shear loading: Soils and Foundations, **18**, 39-56.

Jenkins, S. D., M. W. Waite, and M. F. Bee, 1997, Time-lapse monitoring of the Duri Steamflood: A pilot and study case: The Leading Edge, **16**, 1267–1273.

Johnston, D. H., 1987, Physical properties of shale at temperature and pressure: Geophysics, **52**, 1391–1401.

Johnston, D. H., and M. N. Toksöz, 1981, Definitions and terminology: In: Seismic wave attenuation (Johnston and Toksöz, Eds.), Geophysics reprint series, SEG, Tulsa.

Johnston, D. H., M. N. Toksöz, and A. Timur, 1979, Attenuation of seismic waves in dry and saturated rocks: II. Mechanisms: Geophysics, **44**, 691–711.

Johnston, J. E., and N. I. Christensen, 1995, Seismic anisotropy of shales: J. Geophysical Res., **100**, 5991–6003.

Lesueur, D., and J. F. Gerard, 1996, A structure-related model to describe asphalt linear viscoelasticity: Journal of Rheology, **40**, 813–836.

Macrides, C. G., and E. R. Kanasewich, 1987, Seismic attenuation and poisson's ratios in oil sands from crosshole measurements: J. Can. Soc. Expl. Geophys., **23**, 46–55.

Mah, M., 2005, Determination of elastic constants of orthorhombic and transversely isotropic materials: Experimental application to a kerogen rich rock: Ph.D. thesis, University of Alberta.

Mavko, G., and A. Nur, 1975, Melt squirt in the asthenosphere, J. Geophysical Res., **80**, 1444–1448.

Nur, A., C. Tosaya, and D. Vo-Thanh, 1984, Seismic monitoring of thermal enhanced oil recovery processes: 54th Annual International Meeting, SEG, Expanded Abstracts, 337–340.

O'Connell, R. J., and B. Budiansky, 1977, Viscoelastic properties of fluid-saturated cracked solids: J. Geophysical Res., **82**, 5719–5735.

O'Connell, R. J., and B. Budiansky, 1978, Measures of dissipation is viscoelastic media: Geophysical Research Letters, **5**, 5–8.

Parker, R. D., 1968, The effect of kerogen content on ultrasonic velocities in oil shales: Masters thesis, University of Texas at Austin.

Rawlings, J. O., S.G. Pantula, and D. A. Dickey, 1998, Applied regression analysis - A research tool: Springer texts in statistics (second edition).

Roylance, D., 2001, Engineering viscoelasticity: Course notes, Massachusetts Institute of Technology.

Schmitt, D. R., 1999, Seismic attributes for monitoring of a shallow heated heavy oil reservoir: A case study: Geophysics, **64**, 368–377.

Thomsen, L., 1986, Weak elastic anisotropy: Geophysics, **51**, 1954–1966.

Thomsen, L., 2002, Understanding seismic anisotropy in exploration and exploitation: Distinguished Instructor Short Course (DISC), No. 5, SEG and EAGE.

Tsvankin, I., 2005, Seismic signatures and analysis of reflection data in anisotropic media: Elsevier Science Publ. Co., Inc (second edition).

Tutuncu, A. N., A. L. Podio, A. R. Gregory, and M. M. Sharma, 1998, Nonlinear viscoelastic behavior of sedimentary rocks, Part I: Effect of frequency and strain amplitude: Geophysics, **63**, 184–194.

Vernik, L., and X. Liu, 1997, Velocity anisotropy in shales: A petrophysical study: Geophysics, **62**, 521–532.

Vernik, L., and A. Nur, 1992, Ultrasonic velocity and anisotropy of hydrocarbon source rocks: Geophysics, **57**, 727–735.

Vo-Thanh, D., 1990, Effects of fluid viscosity on shear-wave attenuation in saturated sandstones: Geophysics, **55**, 712–722.

Walsh, J. B., 1966, Seismic wave attenuation in rock due to friction: J. Geophysical Res., **71**, 2591–2599.

Walsh, J. B., 1968, Attenuation in partially melted material: J. Geophysical Res., **73**, 2209–2216.

Walsh, J. B., 1969, New analysis of attenuation in partially melted material: J. Geophysical Res., **74**, 4333–4337.

Watson, I. A., K. F. Brittle, and L. R. Lines, 2001, Heavy-oil reservoir characterization using elastic wave properties: CREWES Research Report, **13**, 777–784.

Winkler, K., A. Nur, and M. Gladwin, 1979, Friction and seismic attenuation in rocks: Nature, **277**, 528-531.

Zhu, Y., and I. Tsvankin, 2006, Plane-wave propagation in attenuative TI media: Geophysics, in print.

APPENDIX A: CONFIDENCE INTERVALS FOR THE COLE-COLE NONLINEAR MODEL

One way of determining the validity of a model (Cole-Cole model in our case) fit to the observed data is to construct confidence intervals. We follow the procedure described by Rawlings et. al. (1998) to construct confidence intervals for fitting models nonlinear in the parameters.

For a normal distribution of errors ϵ (difference between the model and observations), Gallant (1987) shows that

$$\hat{\theta} \quad \dot{\sim} \quad N[\theta, (\mathbf{F}'\mathbf{F})^{-1}\sigma^2], \tag{A1}$$

where θ is the vector of p (p=4 for Cole-Cole model) model parameters, $\hat{\theta}$ is the least squares estimate of θ, the symbol $\dot{\sim}$ denotes "approximately distributed", N denotes normal distribution, $\mathbf{F}$ is the $n \times p$ matrix of partial derivatives (n being the number of data points), and σ is the standard deviation in errors ϵ. $\mathbf{F}(\theta)$ can be computed as $\mathbf{F}(\hat{\theta})$, and σ can be estimated from $s^2(\hat{\theta}) = SS[Res(\hat{\theta})]/(n-p)$ ($SS[Res(\hat{\theta})]$ being the sum of the suqares of the residuals), which gives the estimated variance-covariance matrix for $\hat{\theta}$ as

$$\mathbf{s}^2(\hat{\theta}) \quad = \quad (\mathbf{F}'\mathbf{F})^{-1}s^2. \tag{A2}$$

For the Cole-Cole model (equation 17), the partial derivatives are

$$\frac{\partial \tilde{G}(\omega)}{\partial G_\infty} \quad = \quad 1 - \frac{1}{1+(i\omega/\omega_r)^\alpha}, \tag{A3}$$

$$\frac{\partial \tilde{G}(\omega)}{\partial G_0} \quad = \quad \frac{1}{1+(i\omega/\omega_r)^\alpha}, \tag{A4}$$

$$\frac{\partial \tilde{G}(\omega)}{\partial \omega_r} \quad = \quad \frac{(G_\infty - G_0)i\omega(\frac{i\omega}{\omega_r})^{(-1+\alpha)}\alpha}{(1+(i\omega/\omega_r)^\alpha)^2\omega_r^2}, \tag{A5}$$

$$\frac{\partial \tilde{G}(\omega)}{\partial \alpha} \quad = \quad \frac{(G_\infty - G_0)(\frac{i\omega}{\omega_r})^\alpha Log[\frac{i\omega}{\omega_r}]}{(1+(i\omega/\omega_r)^\alpha)^2}. \tag{A6}$$

Confidence intervals for any other nonlinear function $h(\theta)$ can be calculated from $h(\hat{\theta})$, which is approximately normally distributed with mean $h(\theta)$ and variance $\mathbf{H}(\mathbf{F}'\mathbf{F})^{-\mathbf{1}}\mathbf{H}'\boldsymbol{\sigma}^{\mathbf{2}}$ (Gallant, 1987), where $\mathbf{H}$ is the partial derivative matrix of $h(\theta)$ with respect to the p model parameters. The variance of $h(\hat{\theta})$ can be estimated by

$$\mathbf{s}^2[h(\hat{\theta})] \quad = \quad [\hat{\mathbf{H}}(\hat{\mathbf{F}}'\hat{\mathbf{F}})^{-\mathbf{1}}\hat{\mathbf{H}}']s^2. \tag{A7}$$

The approximate $100(1-\alpha)\%$ confidence interval estimate of $h(\theta)$ is given as

$$h(\hat{\theta}) \pm t_{[\alpha/2,(n-p)]}[\hat{\mathbf{H}}(\hat{\mathbf{F}}'\hat{\mathbf{F}})^{-\mathbf{1}}\hat{\mathbf{H}}'s^2]^{1/2}, \tag{A8}$$

where, t is the Student's t distribution. If the functions of interest are the n values of $\hat{Y}_i$ (the measured values), then $\mathbf{H}(\hat{\theta}) = \mathbf{F}(\hat{\theta})$ (Rawlings et. al, 1998), which is for example the case in Figures 10a-c. For functions of interest other than the n values of $\hat{Y}_i$ (seen in Figure 10d for instance), we need to compute $\mathbf{H}(\hat{\theta})$ for the additional functions of interest.